UNIVERSITÀ DEGLI STUDI DI PADOVA

Dipartimento di Ingegneria Industriale DII

Dipartimento di Ingegneria Industriale

Corso di Laurea Magistrale in Ingegneria Aerospaziale

Design of a Tethered Mission to Saturn with Optimized Trajectory

Relatore: Enrico Lorenzini

Correlatore: Jesús Peláez Álvarez (Universidad Politécnica de Madrid)

Laureando: Riccardo Calaon

Matricola: 1159863

Anno Accademico 2018/2019

Contents

Introduction

The exploration of the outer regions of our Solar System has recently been met by a growing interest from the scientific community worldwide. Several missions so far have flown by all of the gas giants: *Voyager 1* flew past Jupiter and Saturn; *Voyager 2* flew past Jupiter, Saturn, Uranus and Neptune. The *New Horizons* mission made it all the way to Pluto and beyond. Even of greater importance for planetary exploration were the *Galileo* and *Cassini* missions, envisioned to explore the planetary systems of Jupiter and Saturn respectively. These two missions allowed to take a very close look at the planets and their inner characteristics such as their magnetosphere and surface composition, but most interestingly they involved subsequent flybys of the moons of both the planets, paving the way for the chapter of space exploration that is to be written over the next decade. Following the wake of these two missions, both NASA and ESA have set the exploration of planetary systems as a priority for the years to come: NASA's *Europa Clipper* mission is expected to begin in the first half of the 2020s, and will mostly consist in repeated flybys of the jovian moon Europa to study its glacial surface [1]; the Jupiter Icy Moons Explorer (JUICE), by ESA, is planned for launch in 2022 and will investigate Jupiter's atmosphere and magnetosphere together with repeated flybys of the moons Europa, Ganymede and Callisto [2]. The interest in exploring gas giants is motivated by the necessity of understanding the evolution of such celestial bodies and the systems associated with them, in the perspective of future research of exoplanets. Moreover, elaborations

of the data collected so far during past missions have shown that planetary moons, while being covered by a thick layer of ice, might be concealing major bodies of liquid water in the form of internal oceans. For this reason, one of the main goals of such missions is to prove the existence of said oceans and investigate the *habitability* of the moons, which in this specific context means to investigate the moon's suitability to hosting microorganisms similar to those known and existing on Earth [1]. While missions are already being developed to reach Jupiter, another good candidate for the same purposes is the gas giant Saturn. Plumes of water vapor and ice have been observed to be emitted from the souther pole of the saturnian moon Enceladus and to be the main source of matter for the planet's the E-ring [3]. The analysis of the composition of said particles, operated by the Cassini spacecraft, concur with the theory of an inner ocean, below Enceladus's rocky surface and in direct contact with its rocky core [3]. Other studies forecast the presence of a liquid, salty-water ocean underneath the surface of Saturn's largest moon Titan, but analyses conducted so far are more speculative and lack empiric proof [4].

The purpose of this work will be to provide the preliminary orbital design of a mission to explore Saturn and, subsequently, its moons. The aim will also be to explore new techniques, made available by modern technologies, to achieve the mission's goals in a more cost-efficient and better-performing way, in comparison to other planetary missions realized in the past.

Chapter 1

Problem statement

Interplanetary missions are highly complicated and articulated to design, especially when compared with Earth-missions and satellites, due to the high energy required to send a spacecraft outside of the Earth's own gravity field and towards other planets in the deep space. In this section we will analyze some of the most basic key features of an interplanetary mission, without diving too much into the details, but providing satisfactory notions about the physics of the problem and the orders of magnitudes involved. Let's begin by saying that planets' orbits are elliptical and have nonzero inclinations with respect to the Sun's equatorial plane; however, eccentricities and inclinations of the planets are very small and neglecting them (which means assuming planetary orbits to be circular, planar and Sun-centered) allows to speed up early stages of computation obtaining results that are still accurate in the terms of the orders of magnitude involved [5]. For this reason we will, for the moment, assume that planetary orbits are circular, with a heliocentric radius equivalent to the planet's semimajor axis. The planets' linear velocities and orbital energies can be calculated as follows:

$$E = -\frac{\mu_{Sun}}{2r}$$

$$v = \sqrt{\frac{\mu_{Sun}}{r}}$$

	Radius $[km]$	**Velocity** $[km/s]$	**Energy** $[km^2/s^2]$
Mercury	$5.791 \cdot 10^7$	47.872	-1145.87
Venus	$1.082 \cdot 10^8$	35.021	-613.22
Earth	$1.496 \cdot 10^8$	29.785	-443.56
Mars	$2.279 \cdot 10^8$	24.129	-291.11
Jupiter	$7.783 \cdot 10^8$	13.058	-85.25
Saturn	$1.427 \cdot 10^9$	9.645	-46.51
Uranus	$2.870 \cdot 10^9$	6.799	-23.12
Neptune	$4.498 \cdot 10^9$	5.432	-14.75

Table 1.1: Radius, velocity and orbital energy of the planets of the Solar System

1.1 The Hohmann Transfer

1.1.1 Generalities

The *Hohmann Transfer* is the most efficient maneuver, in terms of propellant consumption, to move a spacecraft from a lower circular orbit to a higher circular orbit, or viceversa [5]. As a known result from Tsiolkovsky's equation, the propellant mass required for a certain maneuver increases exponentially with the magnitude of the $\Delta\vec{v}$ to be provided to the spacecraft, according to the law:

$$\Delta m = m_{S/C}\left(exp\left(\frac{\Delta v}{g_0 I_{sp}}\right) - 1\right)$$

Since carrying a high amount of fuel mass into space is expensive, it is necessary to minimize the fuel consumption by minimizing the $\Delta\vec{v}$ that needs to be provided: this is done through the Hohmann maneuver. The optimal transfer orbit is tangent to both the inner and outer orbit, with its periapse coinciding with the inner orbit's radius and its apoapse with the outer orbit's.

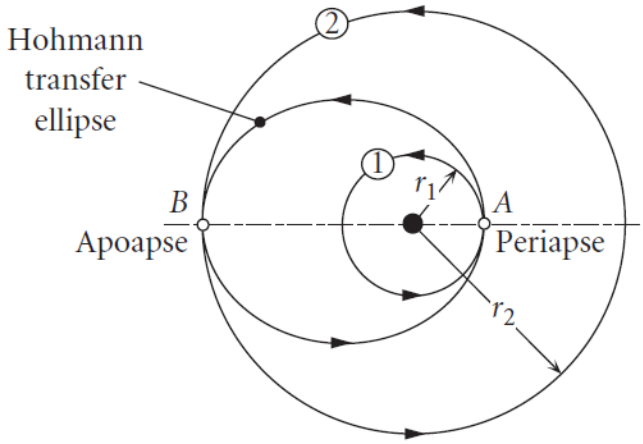

Figure 1.1: Hohmann transfer [6]

A complete Hohmann maneuver consists in two impulses, both fired in the direction of the satellite's velocity: the first one puts the satellite onto the elliptic transfer orbit, the second one circularizes the orbit once the satellite has reached the desired altitude. The equations for the total $\Delta\vec{v}$ required are the following:

$$a_H = \frac{r_1 + r_2}{2}$$

$$\Delta v = \left| \sqrt{\mu \left(\frac{2}{r_1} - \frac{1}{a_H} \right)} - \sqrt{\frac{\mu}{r_1}} \right| + \left| \sqrt{\mu \left(\frac{2}{r_2} - \frac{1}{a_H} \right)} - \sqrt{\frac{\mu}{r_2}} \right|$$

1.1.2 Interplanetary Hohmann Transfer

In the case of an interplanetary transfer, the formulation needs additional development. It is not possible to launch a spacecraft directly into a heliocentric elliptic orbit around the Sun: the spacecraft needs to be put on a parking orbit around the Earth, and subsequently moved into a hyperbolic orbit to exit the Earth's *sphere of influence* with the desired velocity. Let's assume we want to send a spacecraft to Mars: subscripts 'E' refer to

the Earth and 'M' to Mars. The $\Delta\vec{v}$ that the launcher needs to provide is calculated as follows:

$$A_H = \frac{R_E + R_M}{2}$$

$$v_\infty = \sqrt{\mu_{Sun}\left(\frac{2}{R_E} - \frac{1}{A_H}\right)} - \sqrt{\frac{\mu_{Sun}}{R_E}}$$

$$\Delta v_{launcher} = \sqrt{\frac{2\mu_E}{r_p} + v_\infty^2} - \sqrt{\frac{\mu_E}{r_p}}$$

with r_p being the radius of the parking orbit around the Earth and A_H the semimajor axis of the elliptic transfer orbit around the Sun. The following constants are known:

- $\mu_{Sun} = 1.32712440018 \cdot 10^{11}$ km^3/s^2
- $\mu_E = 398600.3$ km^3/s^2
- $r_p = 6678$ km (h=300 km, design parameter)

Assuming that we want to send a spacecraft onto an elliptic heliocentric orbit with a given apoapse (A_H), the Δv required by the launcher is visualized in the green curve in the plot in fig. 1.2. The red curve expresses the sum of the $\Delta v_{launcher}$ and the v_∞ at the sphere of influence of a hypothetical planet whose heliocentric radius equals the given apoapse. When intersecting the destination planet a similar problem arises: it is in fact necessary to define a hyperbolic trajectory around that planet at whose periapse a Δv is required to move the spacecraft into a closed orbit, in order for it to stay captured into the planet's sphere of influence. For a constant value of the periapse radius, the magnitude of the $\Delta v_{capture}$ increases monotonically with v_∞. Even though the graphs shown are qualitative, some interesting notions can be extrapolated:

- the cost of launching a spacecraft to another planet increases with the module of the difference between the planet's radius and the Earth's own radius

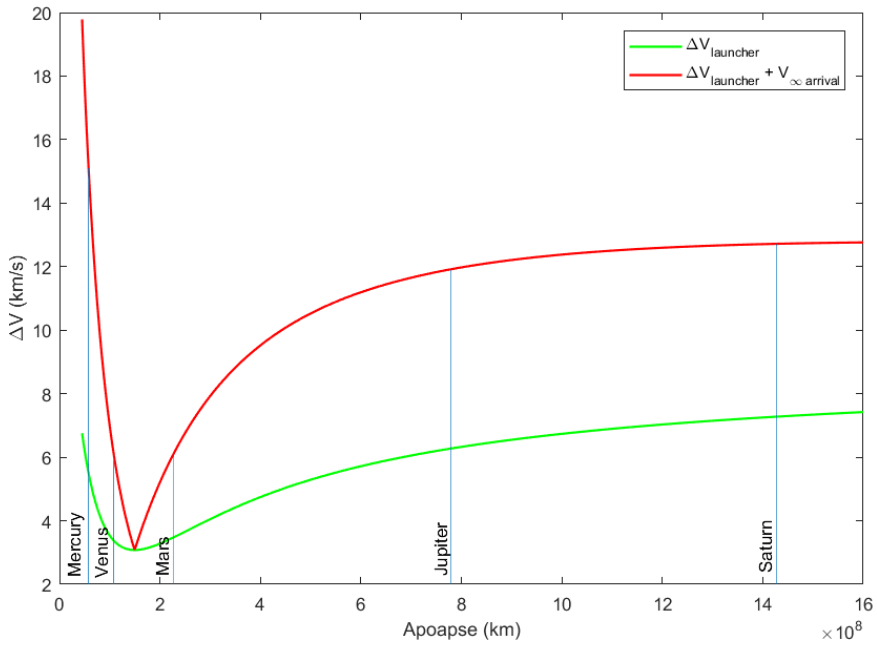

Figure 1.2: Δv's as function of the required apoapse

- a second variable to keep in mind is the v_∞ at the sphere of influence of the destination planet, which might give rise to a fuel-demanding planetary capture.

This second aspect in particular requires alternative approaches for the mission design, in order to decrease the relative speed between spacecraft and planet: the most common strategy involves performing a *Planetary Flyby* which, as will be explained in the details in the following chapters, allows to increase considerably the semimajor axis of the transfer orbit, decreasing the relative speed between the spacecraft and the target planet.

Once the interplanetary transfer orbits have been defined, the hyperbolic trajectories within the planetary spheres of influence are to be defined. The

known parameters are:

- $v_\infty = |\vec{\boldsymbol{v}}_P - \vec{\boldsymbol{v}}_S|$ as previously calculated;
- r_P : periapse; it is a design parameter and can be chosen freely, with the only obvious necessity that it be higher than the planet's equatorial radius to avoid impact. Different choices for r_P only slightly affect the total Δv required.

The other parameters to describe the trajectory are calculated as follows:

- $a = \frac{\mu}{v_\infty^2}$: semimajor axis of the hyperbola;
- $s = \sqrt{r_P\,(r_P + 2a)}$: impact parameter, distance between the planet's center of mass and the asymptotes of the hyperbola
- $\alpha_0 = \arctan\left(\frac{s}{a}\right)$: angle between the asymptotes and the hyperbola's focal axis
- $\delta = \pi - 2\alpha_0$: turn angle of the asymptotes.

1.2 Flyby

A *Flyby*, also known as *Gravity Assist*, is a commonly used strategy in interplanetary mission design, because it can provide the satellite with a $\Delta\vec{\boldsymbol{v}}$ without any propellant consumption. It allows therefore to reach areas of the deep space that would not be achievable with state of the art propulsion systems alone. Considering for example a satellite performing a flyby around a planet of the inner Solar System, it is possible to characterize four different orbits:

- pre-flyby elliptic orbit of the satellite around the Sun;
- elliptic orbit of the planet around the Sun;

- hyperbolic orbit of the satellite around the selected planet;
- post-flyby elliptic orbit of the satellite around the Sun.

In the current analysis we are referring to the method of the *patched conics*, according to which the orbits of the satellite (pre- and post-flyby) around the Sun and the orbit around the planet are joined at the border of the planet's *sphere of influence* (SOI), within which the planet is considered to be the only gravity-field center, while outside of it the gravity center is the Sun. Thanks to this approximation, which is good for a preliminary analysis, it is possible to evaluate different two-body problems separately, for which analytical solutions are provided. While referring to the orbits around the Sun, it is safe to assume that the planetary sphere of influence coincides with the planet itself, due to the radius of the SOI being several orders of magnitude smaller than the other lengths involved. One approximation of the radius of the sphere of influence is the following, in which m_s is the mass of the Sun, m_p that of the planet and R the distance between the planet and the Sun [6]:

$$r_{SOI} = R\left(\frac{m_p}{m_s}\right)^{\frac{2}{5}}$$

Once the intersection with the planet's orbit has been found, it is necessary to calculate the $\Delta\boldsymbol{v} = \vec{\boldsymbol{v}}_S - \vec{\boldsymbol{v}}_P$ which corresponds to the hyperbolic excess velocity of the planetary orbit $\vec{\boldsymbol{v}}_{\infty 1}$. The planetary orbit is usually expressed in a bidimensional frame with the first axis pointing along the planet's velocity (in the approximation of circular orbit) and the second axis pointing at the Sun. With θ being the planet's true anomaly, the directions of the local frame of reference are:

$$\begin{cases} \vec{\boldsymbol{w}}_1 = -\sin\theta\hat{\boldsymbol{i}} + \cos\theta\hat{\boldsymbol{j}} \\ \vec{\boldsymbol{w}}_2 = -\cos\theta\hat{\boldsymbol{i}} - \sin\theta\hat{\boldsymbol{j}} \end{cases}$$

In this example we are assuming that the orbits lie on the same plane, therefore the flyby will also happen on the same plane, making it possible to

neglect the out-of-plane components of vectors. The parameters of the hyperbolic trajectory around the planet are calculated just as explained in the previous chapter. There is one additional degree of freedom depending on the position of entry into the sphere of influence: the flyby can, in fact, be performed on the Sun side or on the shaded side. In one case the angular moment of the hyperbolic trajectory is opposed to that of the planet's orbit around the Sun, and lies on the negative z-semiaxis of the local frame; in the other case they point at the same direction, with the angular moment lying on the positive z-semiaxis. Once determined wether the flyby happens on the shaded side or on the Sun side, it is possible to calculate the positions of the perigee in the local frame and the direction of the outbound velocity. Defining ϕ_1 and ϕ_2 the directions of inbound and outbound $\vec{\boldsymbol{v}}_\infty$ we have:

Positive angular moment	Negative angular moment
$\beta = \phi_1 - \alpha_0$	$\beta = \phi_1 + \alpha_0$
$\vec{\boldsymbol{r}}_p = r_p\{\cos\beta, \sin\beta\}$	$\vec{\boldsymbol{r}}_p = r_p\{\cos\beta, \sin\beta\}$
$\phi_2 = \phi_1 + \delta$	$\phi_2 = \phi_1 - \delta$
$\vec{\boldsymbol{v}}_{\infty 2} = v_\infty\{\cos\phi_2, \sin\phi_2\}$	$\vec{\boldsymbol{v}}_{\infty 2} = v_\infty\{\cos\phi_2, \sin\phi_2\}$

Once the outbound velocity is known, it will suffice to express it in inertial coordinates and add it to the planet's velocity to obtain the satellite's post-flyby velocity.

$$\vec{\boldsymbol{v}}_{s2} = \vec{\boldsymbol{v}}_p + \vec{\boldsymbol{v}}_{\infty 2}$$

In first-order approximation, the position of the satellite will be the same it was occupying before the flyby, which also coincides the planet's position at the intersection point. Knowing the position and the new velocity of the satellite means knowing its state vector, from which it is possible to fully determine the post-flyby orbit of the satellite.

1.3 Cassini's designed trajectory

To provide an example of what has been explained so far, we present the pre-launch design of Cassini's trajectory. The trajectory consisted in a VVEJGA-1DSM scheme, whose specifics can be read in table 1.2. Together with planetary flybys and the DSM between the subsequent flybys of Venus, the preliminary desing accounted for 22 *trajectory correction maneuvers* (TCM); more specifically, TCM-1 was implemented to correct launch errors, while TCM-9 through TCM-12 were to correct an Earth-bias deliberately built into the trajectory to ensure a probability of impact with the Earth lower than 10^{-6} [7]. The overall trajectory, from launch to arrival at Saturn is visualized in fig 1.3.

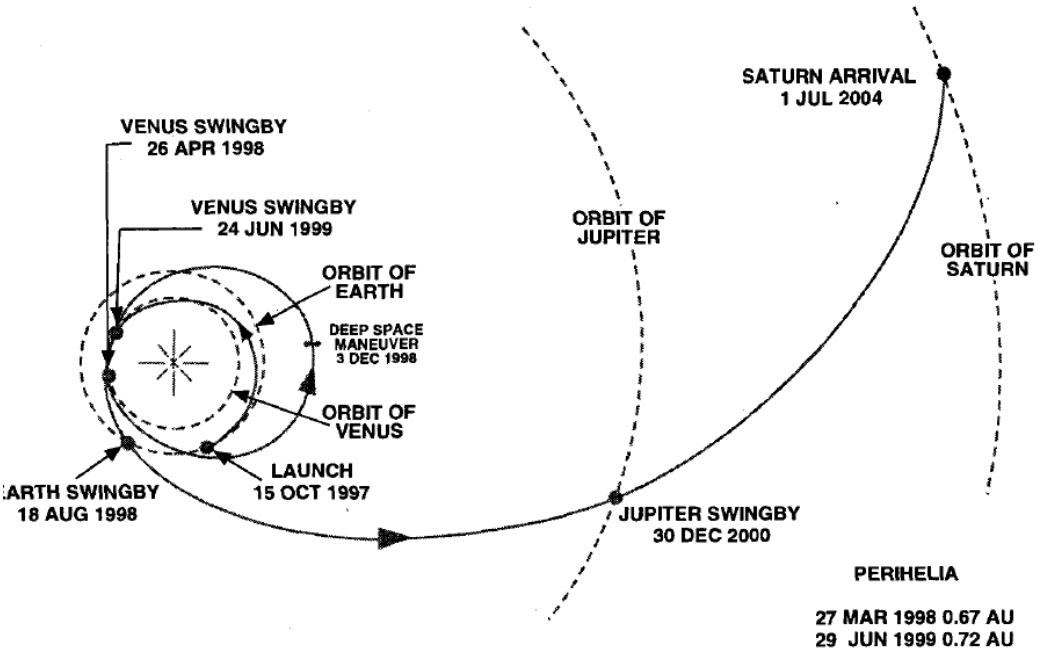

Figure 1.3: Cassini's designed trajectory [7]

Event	**Date**	**s** $[km]$	**Δv** $[m/s]$
Launch	15 Oct 1997	/	/
TCM-1	30 Oct 1997	/	1.4
Venus-1 Flyby	26 Apr 1998	12302	/
DSM	3 Dec 1998	/	451.8
Venus-2 Flyby	24 Jun 1999	-9084	/
TCM-9 (V+10d)	4 Jul 1999	-9084	42.3
TCM-10 (E-30d)	19 Jul 1999	57510	4.9
TCM-11 (E-15d)	3 Aug 1999	10390	36.9
TCM-12 (E-6.5d)	11 Aug 1999	8954	13.0
Earth Flyby	18 Aug 1999	8954	/
Jupiter Flyby	30 Dec 2000	10896274	/
Saturn Encounter	1 Jul 2004	393160	/

Table 1.2: Major events in Cassini's designed trajectory [7]

Chapter 2

Optimization Algorithms

The problem of finding good and feasible launch windows when designing an interplanetary mission is just as articulated as it is imprescindible. The complexity is represented by the high number of independent variables involved in the computation, together with the non-linearity of the problem and with the impossibility of knowing *a priori* whether, for a given set of the independent variables, a solution exists or not. The best approach to an optimization problem begins therefore with the definition of a *cost function* [8], through which it is possible to directly evaluate the "goodness" of a certain combination of variables: when designing an interplanetary mission the cost function is usually given by the cumulative $\Delta\vec{v}$ to be provided to the spacecraft to reach its final destination. The problem turns into finding the minimum value of the cost function over a multidimensional domain. When the function is non-linear and non-differentiable, direct search methods are to be implemented [8], which require to explore the domain in an iterative search for best-fitting solutions. The requirements for an optimization algorithm of this style can be summarized in the following four points [8]:

1. Ability to handle non-linear and multivariable functions

2. Parallelizability, in case of high computational costs demanded by fre-

quent cost function evaluations

3. Easy choice of the independent variables of the problem

4. Good convergence properties.

2.1 Differential Evolution

2.1.1 General concepts

Differential Evolution is an algorithm that involves NP D-dimensional vectors:

$$x_{i,G} \text{ for } i = 1, 2, ..., NP$$

with NP being the number of individuals (vectors) belonging to the G-th generation and D the number of independent variables. A problem characterised by 5 variables will therefore involve 5-dimensional individuals. The initial generation ($G = 0$) can be generated randomly or, in case the position of an optimal solution were known in advance with a certain error, the initial generation can be created by adding to that solution a distribution of randomly generated deviation vectors [8]. The Differential Evolution Algorithm belongs to a class named *Evolutionary Algorithms*, which get their name from being inspired by the way evolution happens with living species. With this idea in mind, the code will proceed creating subsequent generations of individuals through the operations known as *mutation*, *crossover* and *natural selection*.

- **mutation**: for each i-vector of the G-th generation, a mutant vector $v_{i,G+1}$ is generated as a linear combination of other vectors according to the following relation: [8]

$$v_{i,G+1} = x_{r1,G} + F(x_{r2,G} - x_{r3,G})$$

where G is a positive integer indicating the generation to which the vectors belong, $r1 \neq r2 \neq r3 \neq i$ are also integers and F, the *mutation factor*, is a real value that usually lies in the interval $[0.4, 1]$ and controls the length of the exploration vector $(x_{r2,G} - x_{r3,G})$ [9]

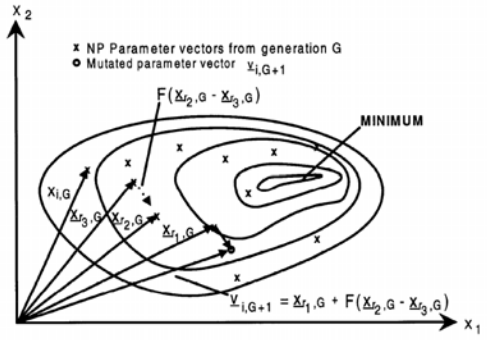

Figure 2.1: Generation of mutant vector in a 2D domain [8]

- **crossover**: to increase the diversity of the parameter vector [8] the crossover operation has it inherit at least one parameter from the mutant vector. With this purpose *trial vector* $u_{i,G+1}$ is defined as follows [8]:

$$u_{i,G+1} = \begin{cases} v_{i,G+1} & \text{if } randb(j) \leq CR \text{ or } j = rnbr(i) \\ x_{i,G+1} & \text{if } randb(j) > CR \text{ and } j \neq rnbr(i) \end{cases} \quad \text{for } j = 1, ..., D$$

  In the previous formula, $randb(j) \in [0, 1]$ is a random real number defined for every j-th component, while $CR \in [0, 1]$ is the *crossover parameter*, which regulates the probability for the $v_{i,G+1}$ vector to pass a parameter on to the next-generation vector. The integer $rnbr(i) \in [1, D]$ makes sure that at least one parameter of the trial vector $u_{i,G+1}$ is inherited from $v_{i,G+1}$.

- **natural selection**: this last step evaluates the cost function for the trial vector $u_{i,G+1}$ so far calculated. If it produces a lower (or better

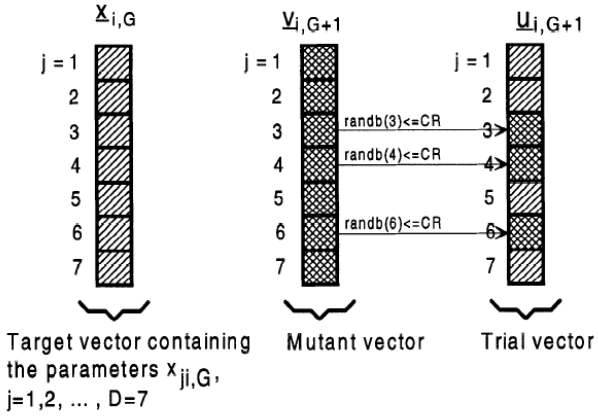

Figure 2.2: Crossover operation with a 7D parameter vector [8]

performing) cost value, the vector $u_{i,G+1}$ becomes the i-th member of the generation G+1; if not, the vector $x_{i,G}$ is passed on to the next generation instead.

The scheme proposed so far is the most basic and the first one that has been developed. There exist different variants, whose efficiencies need to be tested, since usually there appears to be no rule to determine which one works best. Different implementation options involve an alternative formulation for the mutation procedure. The one previously defined is defined *DE/rand/1*, other options are the following [10]:

- *DE/rand/2*: $v_{i,G+1} = x_{r1,G} + F(x_{r2,G} - x_{r3,G}) + F(x_{r4,G} - x_{r5,G})$
- *DE/best/1*: $v_{i,G+1} = x_{best,G} + F(x_{r1,G} - x_{r2,G})$
- *DE/current to best/1*: $v_{i,G+1} = x_{i,G} + F(x_{best,G} - x_{i,G}) + F(x_{r1,G} - x_{r2,G})$
- *DE/best/2*: $v_{i,G+1} = x_{best,G} + F(x_{r1,G} - x_{r2,G}) + F(x_{r3,G} - x_{r4,G})$

Other optimization techniques have been investigated. It can be proved, both experimentally and analytically, that the convergence properties of the

Differential Evolution algorithm strongly depend on user-defined parameters such as *F, CR* and *NP* [9]. As far as the population number, the general rule of thumb recommended by Storn and Price is to choose $NP \in [5D, 10D]$; nevertheless it is important, for the mutation operation to be successful, that there be at least four or more elements in the population, according to the mutation strategy adopted [8]. The choices for the F and CR parameter affect the convergence speed of the algorithm: $CR \approx 1$ is usually an inappropriate choice, but good for a preliminary search of possible solutions [8]. If the solution converges too quickly, it might be useful to increase the value of F to force the code into looking for solutions farther away from the parent vectors. Since the most appropriate choice for the design parameters usually depends on the problem itself, another subclass of Differential Evolution algorithms has been developed, according to which the design parameters mutate along the code together with the variables of the problem. These are called *Self-Adaptive Algorithms*, and consist in adding two additional components to the element vector, which play the role of the F and CR parameters at each DE iteration. Note that the calculation of new $F_{i,G+1}$ and $CR_{i,G+1}$ is done in advance, and the results are applied to the computation. An example is the following [11]:

$$F_{i,G+1} = \begin{cases} F_l + rand_1 * F_u \text{ if } rand_2 < \tau_1 \\ F_{1,G} \text{ if } rand_2 \geq \tau_1 \end{cases}$$

$$CR_{i,G+1} = \begin{cases} rand_3 \text{ if } rand_4 < \tau_2 \\ CR_{1,G} \text{ if } rand_4 \geq \tau_2 \end{cases}$$

In the previous formulas, $rand_j \in [0, 1]$ is a real number, while suggested values are $F_l = 0.1$ and $F_u = 0.9$ in order to get an $F_{i,G+1} \in [0, 1]$, as it usually happens in most cases, and $\tau_1 = \tau_2 = 0.1$ [11].

2.1.2 Limits and drawbacks

A few comments on the most common drawbacks that can be encountered while applying DE algorithms. *Premature convergence* is a phenomenon that occurs quite frequently and, generally speaking, cannot be avoided actively. It consists in the algorithm converging to a local optimal solution that is however not optimal in the global domain: it is the multidimensional equivalent of encountering a local minimum of a carthesian function, which might not coincide with the global minimum. When a local minimum is encountered the algorithm does not proceed, and the population loses its diversity as each vector tends to be replaced by the local optimum vector. The only way out of local minima is running the algorithm several times, with different randomly-generated initial populations: this way, since the algorithm itself evolves stochastically, once the same set of parameters is encountered as a optimum solution after several runs it can be considered to have good global properties as well.

The problem of *stagnation* is another phenomenon that stalls the algorithm, but happens for a different set of reasons, as investigated thoroughly in [12]: when stagnation occurs the population is still diverse, but the code cannot progress towards a better solution and remains stuck. This is due to the lack of viable combinations of vectors to produce new individuals with a better fitness value, therefore older-generation vectors are passed on to new generations unaltered. When the population number NP is low, there only exists a very limited number of combinations to produce mutant vectors, especially when the mutation factor F is kept constant. Moreover, it can be easily shown that in the case $F = 1$ the number of distinct mutant vectors is reduced by 50% [12], which happens because the same linear combination of vectors is obtained for different $v_{i,G+1}$ calculations: to avoid stagnation, it is therefore recommended to avoid the case $F = 1$. As far as the crossover coefficient, both the cases $CR = 0$ and $CR = 1$ are to be avoided: in the

first, none of the elements of the mutant vector are passed on to the trial vector $u_{i,G+1}$, which will end being identical to the parent $x_{i,G}$; in the latter case, every element of $u_{i,G+1}$ comes from the mutant vector: this way the trial vector does not inherit any data from the parent and falls out of the convergence area, only rarely producing better results.

In conclusion, Differential Evolution Algorithms are a efficient in the process of analyzing multivariable problems, even though attention has to be paid by the user and results need to be evaluated critically. A high population size (NP) increases the diversity of the population itself, reducing both the risks of stagnation and premature convergence, even though larger populations make the whole computation more expensive: a tradeoff in the population size is therefore needed.

2.2 Design Strategies for Multiple Flybys

So far some of the optimization techniques to handle multivariable problems have been investigated; in this section a few examples will be given on how to formulate the problem of designing a space mission which involves multiple gravity assists. Two examples will be presented here: the *Multiple Gravity Assist* (MGA) and *Multiple Gravity Assist with Deep Space Maneuver* (MGA-DSM) [13]. Both methods are based on the *patched conics* approximation theorised by Minovitch and well explained in Curtis [6]; in both cases the planet sequence cannot be optimized by the algorithm, but has to be given by the user as an input. In the examples provided the orbits of the planets are considered to be coplanar, out-of-plane components are therefore neglected; however, simple adjustments allow to apply the same techniques to the problem involving real ephemerides.

2.2.1 Multiple Gravity Assist

The MSA strategy is easier conceptually and faster to implement computationally; however, since it involves a lower number of degrees of freedom, the solutions provided by this method are, generally speaking, less optimal in terms of global cost. The only variables involved are time variables: more specifically, the Δt_i's needed to fly from planet $i-1$ to planet i, for $i = 0, ..., N$. An additional degree of freedom is used: Δt_0 is the *wait time* before launch, meaning the time that has to be waited from the moment in which the planetary ephemerides are given. The indices are given such as:

- $i = 0$: Earth;
- $i = 1, ..., N-1$: flyby planet(s);
- $i = N$: destination planet.

The first step, for a given combination of the variables, is to propagate the orbits of the planets according to the following procedure (note that the planetary ephemerides at $t = 0$ have to be given at the same instant for all the planets):

$$T_i = \sum_{j=0}^{i} \Delta t_j$$

$$[\vec{\boldsymbol{r}}_i(T_i), \vec{\boldsymbol{v}}_i(T_i)] = f\left(\vec{\boldsymbol{r}}_i(0), \vec{\boldsymbol{v}}_i(0), T_i\right)$$

The N transfer orbits are found as solutions to *Lambert's problem*, according to which once two position vectors and the time of flight are given, there only exists one orbit that connects the two positions in the given time of flight [14]. Incoming and outgoing velocity vectors are calculated from the planet's own velocity and the satellite's velocity in the same position but on the transfer orbits [13]:

$$\begin{aligned} \vec{\boldsymbol{v}}_{\infty-in} &= \vec{\boldsymbol{v}}_{S-in} - \vec{\boldsymbol{v}}_P \\ \vec{\boldsymbol{v}}_{\infty-out} &= \vec{\boldsymbol{v}}_{S-out} - \vec{\boldsymbol{v}}_P \end{aligned}$$

The two velocities will in general be different, following two different hyperbolic trajectories around the planet. The aim is to calculate the parameters in order for the two hyperbolic arcs to have the same perigee: the velocity difference between the two orbits will be compensated by an impulse provided by a chemical thruster. The procedure is the following [13], where μ is to be intended as the gravity constant of the current i-th planet:

$$a_{in} = \frac{\mu}{v_{\infty-in}^2}$$

$$a_{out} = \frac{\mu}{v_{\infty-out}^2}$$

The turn angle δ can be calculated from the velocity vectors [13]:

$$\delta = \arccos\left(\frac{\vec{\boldsymbol{v}}_{\infty-in} \cdot \vec{\boldsymbol{v}}_{\infty-out}}{v_{\infty-in} v_{\infty-out}}\right)$$

Once δ has been calculated, the two following equations can be combined into a final single-variable equation [13]:

$$\begin{cases} r_P = a_{in}\left(e_{in} - 1\right) = a_{out}\left(e_{out} - 1\right) \\ \delta = \arcsin\left(\dfrac{1}{e_{in}}\right) + \arcsin\left(\dfrac{1}{e_{out}}\right) \end{cases}$$

$$\left[\frac{a_{out}}{a_{in}}(e_{out} - 1) + 1\right] \sin\left(\delta - \arcsin\left(\frac{1}{e_{out}}\right)\right) - 1 = 0$$

In the last equation the only unknown variable is e_{out}, which can be calculated iteratively. Once calculated, it can be substituted into the other equations to obtain all the parameters. The Δv at perigee is can be calculated as [13]:

$$\Delta v_{fb} = \left| \sqrt{v_{\infty-in}^2 + \frac{2\mu}{r_P}} - \sqrt{v_{\infty-out}^2 + \frac{2\mu}{r_P}} \right|$$

At this point, the only step left is to compute the cost function which will be object of optimization. Naming $\boldsymbol{X}$ the decision vector containing the variables and C the cost function, this leads to [13]:

$$\boldsymbol{X} = [\Delta t_0, ..., \Delta t_N]$$

$$C = f(\boldsymbol{X})$$

In this case, the cost function can simply be the sum of all the $\Delta v_{fb,i}$, when trying to optimize the flybys reducing the fuel consumption and making them as close as possible to a pure unpowered flyby [13]; alternatively, the Δv_{launch} and $v_{\infty,N}$ can be added to the cost, in order to obtain minimum solution in terms of global propellant consumption.

2.2.2 Multiple Gravity Assist with Deep Space Maneuver

The MGA design strategy might not be suitable for all missions, especially when a high number of flybys are necessary. The MGA-DSM strategy consists in performing a deep space maneuver some time after each planetary flyby; the maneuver aims at targeting the next planet in the sequence, and the time at which the maneuver is to be performed is another parameter for the optimization. Therefore there will be a deep space maneuver for each transfer sequence between planets, which in some cases can result in a lower global mission cost [13]. For the launch sequence four parameters need to be defined: the wait time Δt_0, the hyperbolic excess speed v_∞, and right ascension and declination angles α and β. The velocity vector at departure from the Earth is calculated as [13]:

$$\vec{\boldsymbol{v}}_s = \vec{\boldsymbol{v}}_E + v_\infty \left[\cos\alpha\cos\beta\hat{\boldsymbol{i}} + \sin\alpha\cos\beta\hat{\boldsymbol{j}} + \sin\beta\hat{\boldsymbol{k}}\right]$$

As in the MGA strategy, each interplanetary transfer is characterized by a Δt_i, which is the total time of flight from one planet to the following. We define the burn index $\epsilon_i \in [0, 1]$, so that the maneuver will occur at time $\epsilon_i \Delta t_i$ from the last planetary departure. The entity of the Δv will be the modulus of the vectorial difference between the velocity of the satellite before and after the maneuver; the post-maneuver orbit is calculated as the solution to Lambert's problem, which aims at targeting the next planet in a

time equal to $(1 - \epsilon_i)\,\Delta t_i$. In practice, $\epsilon_i = 0$ and $\epsilon_i = 1$ mean applying the DSM at departure and arrival respectively, so a more reasonable choice is $\epsilon_i \in [0.01, 0.99]$ [13]. When each planet is reached, the incoming hyperbolic excess velocity is given, as usual, as the difference between the velocity of the spacecraft and that of the planet. Since the flyby is unpowered, the outgoing velocity will have the same modulus. The degree of freedom for the flyby can be alternatively the periapse radius of the hyperbola r_P or the impact factor s, as explained in the previous sections. The decision vector and cost function, in this case, take the form [13]:

$$\boldsymbol{X} = [\Delta t_0, v_\infty, \alpha, \beta, \Delta t_1, ..., \Delta t_N, \epsilon_1, ..., \epsilon_N, r_{P1}, ..., r_{PN}]$$

$$C = f\,(\boldsymbol{X})$$

Again, the cost function can be modelled to include only the total amount of Δv required by the DSM's, or the hyperbolic excess speed at departure and arrival.

2.2.3 Problem Constraints

In optimization problems constraints are often used to ensure that the final solution is not just theoretically correct, but also practically feasible [13]. Using constraints is preferable because they allow a higher level of smoothness in the evaluation of the cost function, rather than just imposing limits on the domain of the variables involved. In interplanetary mission design, the most common constraints are applied to ensure altitude limits, to keep the satellite from hitting the surface of a planet during a flyby, and low velocity avoidance, to keep the satellite from entering into a low-energy planetary orbit which might lead to planetary capture [13]. Constraints are introduced adding to the cost function C a constraint function G that virtually increases the global cost when the solution is close to one of the risky aforementioned situations.

In the case of altitude limit, an example of a constraint function is [15]:

$$G_1(\boldsymbol{X}) = \sum_{i=1}^{N} -2 \log \frac{r_{pi}}{k R_{Pi}}$$

where r_{pi} is the periapse of the hyperbolic orbit, R_{Pi} is the equatorial radius of the planet and k is a multiplier that can be chosen according to how close the spacecraft can fly to the planet's surface [15], usually $k = 1.05$.
To avoid low velocity flyby, the energy of the planetary orbit is calculated with a 10% uncertainty on the v_∞; this is due to the fact that the planet's sphere of influence is a mathematical abstraction and does not exist in practice. When a closed orbit ($E < 1$) is obtained with $0.9 v_\infty$ a penalty factor is added to the cost function [15]:

$$E_i = \frac{(0.9 v_\infty)^2}{2} - \frac{\mu_P}{R_{SOI}}$$

$$G_2(\boldsymbol{X}) = \sum_{i=1}^{N} \begin{cases} 0 \text{ if } E_i \geq 0 \\ \dfrac{1}{v_{\infty,i}} \text{ if } E_i < 0 \end{cases}$$

2.3 Preliminary Results

Some preliminary solutions where calculated as a base for further analysis for this work. In both cases, the mission consisted in reaching Saturn performing a planetary flyby around Jupiter, to increase the spacecraft's semimajor axis and reduce the relative speed at the encounter with Saturn. The two solutions presented were calculated with the MGA strategy; no constraints were added to the computation, as the results were to be further processed in the following sections of this work. The planetary ephemerides were calculated from the planets' state vectors at a given time, after removing out-of-plane components in order to obtain planar orbits. The keplerian parameters are therefore affected by inaccuracies, and do not account for secular variations

which, in a final analysis, should be included given the long times involved in the mission. This will not affect the validity of the calculations carried out subsequently, as they would only need to be corrected with the real planetary ephemerides. The two solution only differ in the way the cost function was formulated: in the first case a global optimum solution is searched, accounting for the total cost of launch, maneuver and planetary capture; in the secondo case, only the maneuver $\Delta \boldsymbol{v}$ is minimized, resulting in a free Jupiter flyby.

Global optimum: $\Delta \boldsymbol{v}_{tot} = \Delta \boldsymbol{v}_{launch} + \Delta \boldsymbol{v}_{fb} + \boldsymbol{v}_{\infty,S}$

	Earth	**Jupiter**	**Saturn**
encounter date	19/07/2035	28/04/2038	26/10/2047
e	0.01136	0.04589	0.05377
i	0.0	0.0	0.0
ω (deg)	130.100	11.4535	92.003
Ω	/	/	/
θ (rad)	3.0177	1.9407	3.185
a (km)	$1.5194 \cdot 10^8$	$7.7453 \cdot 10^8$	$1.425 \cdot 10^9$

Table 2.1: Orbits of the planets involved

The current orbit sequence is visualized in fig. 2.3 and is obtained with the following $\Delta \boldsymbol{v}$'s:

- $\Delta \boldsymbol{v}_{launch} = 6.304$ km/s;
- $\Delta \boldsymbol{v}_{fb} = -0.3584$ km/s (fired against the spacecraft's speed);
- $\boldsymbol{v}_{\infty,S} = 1.4245$ km/s.

The flyby happens on the sun side. The incoming and outgoing orbits are described in table 2.3:

	Transfer 1	**Transfer 2**
e	0.6729	0.3246
i	0.0	0.0
ω (deg)	302.745	96.2015
Ω	/	/
a (km)	$4.69797 \cdot 10^8$	$1.13382 \cdot 10^9$
$\theta_{departure}$ (rad)	0.00445	0.46159
$\theta_{arrival}$ (rad)	3.1399	3.1117
ΔT (years)	2.78	9.50

Table 2.2: Transfer orbits 1 and 2

	Incoming Flyby	**Outgoing Flyby**
e	1.04882	1.00766
i	0.0	0.0
ω (deg)	156.849[1]	156.849[1]
Ω	/	/
a (km)	$4.217 \cdot 10^6$	$2.687 \cdot 10^7$
r_P (km)	205871	205871

Table 2.3: Flyby orbits

[1]The perigee argument of the flyby orbit is to be intended as the angle measured from Jupiter's transversal velocity component and the position of the periapse of the hyperbolic flyby orbit.

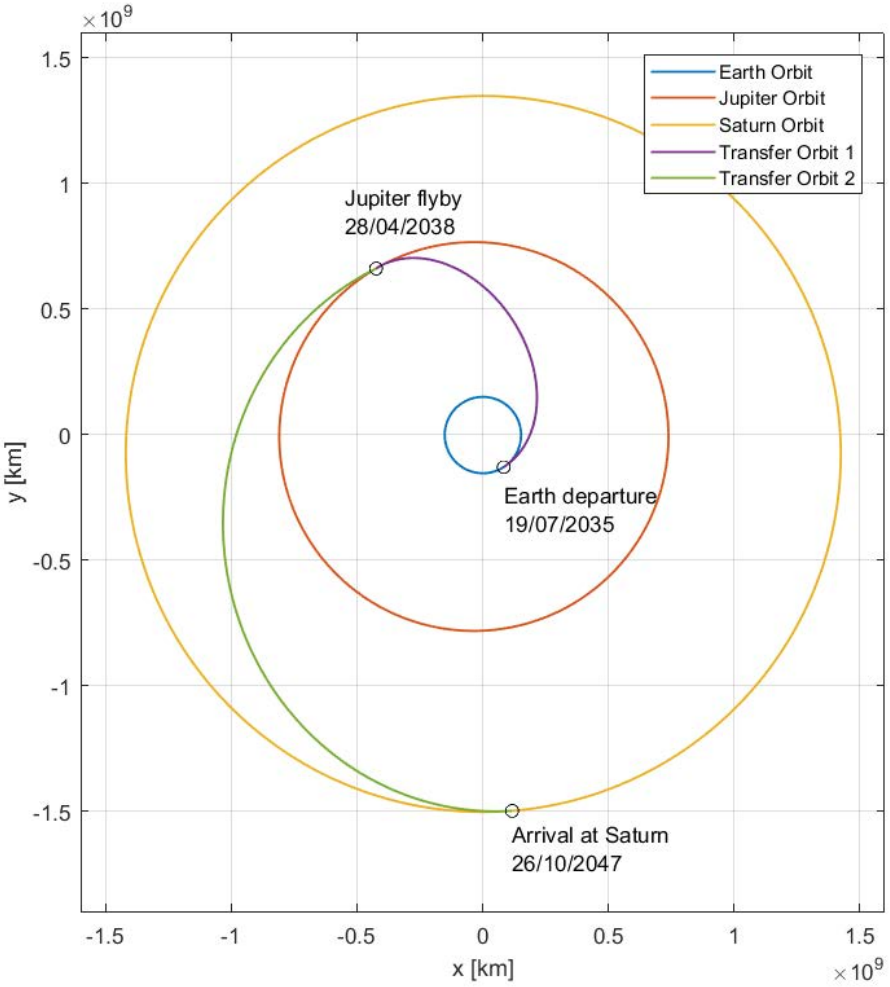

Figure 2.3: Orbit sequence with global optimization

Pure Flyby : $\Delta \boldsymbol{v}_{fb} \to 0$

	Earth	**Jupiter**	**Saturn**
encounter date	13/10/2037	23/03/2040	19/02/2047
e	0.01136	0.04589	0.05377
i	0.0	0.0	0.0
ω (deg)	130.100	11.4535	92.003
Ω	/	/	/
θ (rad)	4.1776	2.8938	3.0540
a (km)	$1.5194 \cdot 10^8$	$7.7453 \cdot 10^8$	$1.425 \cdot 10^9$

Table 2.4: Orbits of the planets involved

	Transfer 1	**Transfer 2**	**Flyby Orbit**
e	0.6880	0.4553	1.6851
i	0.0	0.0	0.0
ω (deg)	5.2134	88.6728	147.244[2]
Ω	/	/	/
a (km)	$4.8935 \cdot 10^8$	$1.0319 \cdot 10^9$	$3.9518 \cdot 10^6$
$\theta_{departure}$ (rad)	0.07414	1.54606	/
$\theta_{arrival}$ (rad)	3.0027	3.1121	/
ΔT (years)	2.44	6.91	/
r_P (km)	/	/	$2.7072 \cdot 10^6$

Table 2.5: Transfer orbits 1 and 2 & Flyby orbit

The current orbit sequence is visualized in fig. 2.4 and is obtained with the following $\Delta \boldsymbol{v}$'s:

[2]The perigee argument of the flyby orbit is to be intended as the angle measured from Jupiter's transversal velocity component and the position of the periapse of the hyperbolic flyby orbit.

- $\Delta \boldsymbol{v}_{launch} = 6.435$ km/s;
- $\Delta \boldsymbol{v}_{fb} = 6.08 \cdot 10^{-12}$ km/s;
- $\boldsymbol{v}_{\infty,S} = 2.2102$ km/s.

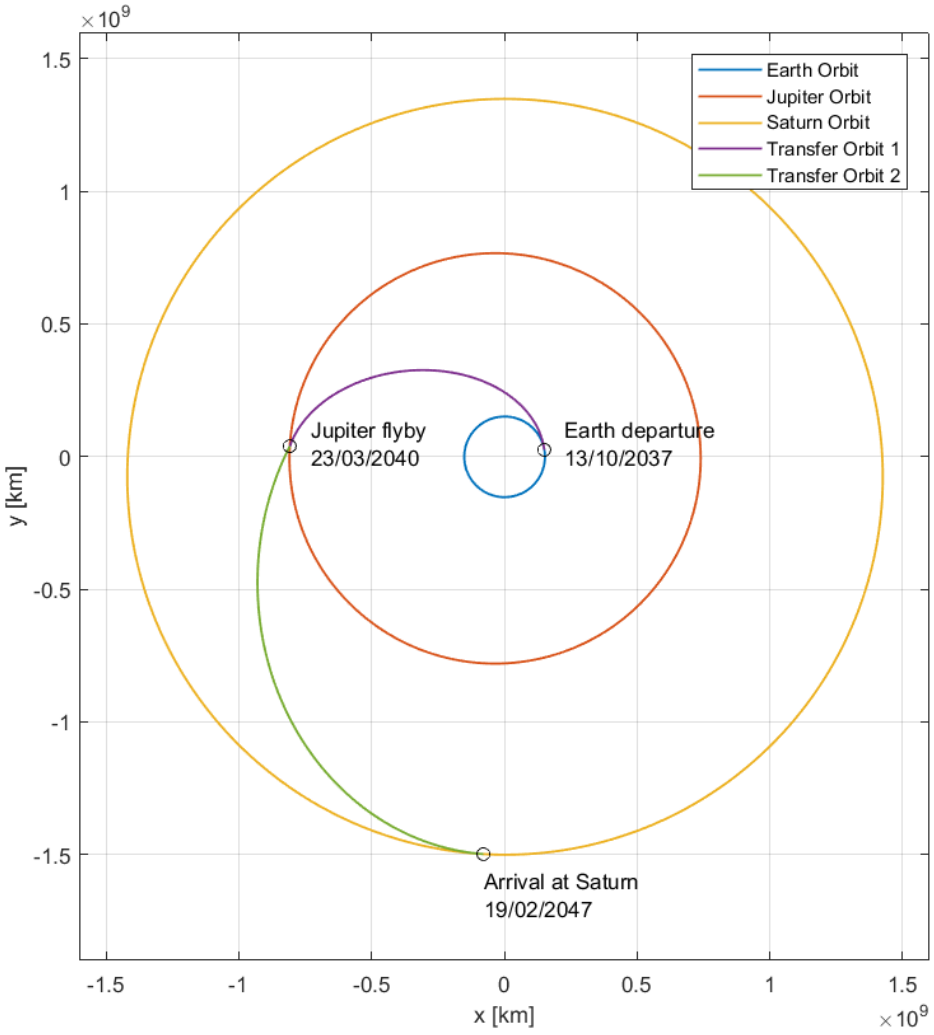

Figure 2.4: Orbit sequence with global optimization

A few basic concepts can be extrapolated from the previous examples. First of all, when implementing a global optimization technique we obtain the best result in terms of total $\Delta \boldsymbol{v}$, but it is not possible to control each of the terms that add up to the sum singularly: this results in a quite high $\Delta \boldsymbol{v}_{fb}$, which would require a considerable fuel burn. When optimizing the global $\Delta \boldsymbol{v}$ the algorithm stabilizes on a solution that is very close to performing two Homann's transfer orbits, with the true anomaly θ going from values close to 0 at departure time to values close to π when approaching the destination: this is only feasible with the additional degree of freedom given by the maneuver at the periapse of the flyby orbit. In the second case, the flyby maneuver is reduced to near-zero value resulting in a free flyby; as a consequence, there is no *a priori* control over $\Delta \boldsymbol{v}_{launch}$ and $\boldsymbol{v}_{\infty,S}$. As far as the first term is concerned, the user will need to prune the solutions in order to find those that grant a $\Delta \boldsymbol{v}_{launch}$ compatible with available launcher technology. The $\boldsymbol{v}_{\infty,S}$ usually falls in the range $[2, 3]$ km/s, depending on the real positions of departure and arrival due to the planets' ellipticity. The maneuver in Jupiter apparently looks beneficial for the final encounter with Saturn, lowering the hyperbolic excess velocity to $\boldsymbol{v}_{\infty,S} = 1.4245$ km/s, which is better than what can usually be accomplished with a pure flyby, but still suffers the high costs required by the maneuver. Tests were run to try to find the solution with the lowest hyperbolic excess speed at Saturn's sphere of influence; the best results obtained were around $\boldsymbol{v}_{\infty,S} \approx 1.3$ km/s, at the expenses of more intense maneuvers in the other phases of the mission: this means that, in order to reduce the relative velocity at the encounter with Saturn, other strategies need to be implemented.

Chapter 3

Optimizing the Capture with Low Thrust

In this chapter the results of the analysis conducted up to this point will be elaborated and perfected. The Cassini Mission reached Saturn with a hyperbolic excess speed of $\boldsymbol{v}_\infty = 5.6$ km/s and, to have the spacecraft captured into the sphere of influence of the planet, a $\Delta v = 622$ m/s was necessary; this required a consumption of 800 kg of propellant [7, 16], which had a severe impact on the mass budget of the mission. Moreover, the spacecraft was put onto a highly elliptic orbit around Saturn, requiring a second maneuver and several subsequent flybys of Saturn's moons to raise its periapse [16]. Since the energy of the hyperbolic orbit entering Saturn's sphere of influence is directly proportional to the parameter $c_3 = \boldsymbol{v}_\infty^2$, reducing the relative speed means facilitating the capture maneuver. In order to do so, a *low-thrust arc* will be inserted in the transfer orbit from Jupiter to Saturn: the low thrust will be provided by an electric thruster; the main parameters involved will be the acceleration α provided by the thruster, the orientation angle β of the thrust vector, the time during which the thruster is turned on T_{thr} and the delay time δ to be waited from the departure from Jupiter before turning on the thruster. The parameters will be chosen according to the performances

of different types of electric thrusters available on the market (ion thrusters, Hall-effect thrusters...) and based on the best fitting parameters obtained by the simulations.

3.1 Gaussian Planetary Equations

The method implemented to obtain the motion of the spacecraft along the thrust arc consists in integrating the *Gaussian Planetary Equations*, which can be derived for each one of the six classical orbital elements through the Variation of Parameters (VoP) technique. First of all, it is necessary to point out that applying a thrust arc for an extended period of time makes it impossible to work with classic keplerian orbits: the spacecraft is subject to non-conservative forces (the thrust) and keplerian theory does not apply. During its motion along the thrust arc the spacecraft will occupy, at each instant, a specific position in space $\vec{\boldsymbol{r}}$ with a certain velocity $\vec{\boldsymbol{v}}$; knowing the state vector allows to calculate the keplerian parameters of the S/C *in that specific instant*: this set of parameters will be called *osculating parameters* and will correspond to an *osculating orbit*, which is a keplerian unperturbed orbit, locally tangent to the spacecraft's motion in the given position.

3.1.1 Variation of Parameters and derivation of the equations

The Variation of Parameters method is based on the idea that the solution to the perturbed system can be described by a sequence of solutions to the unperturbed system, meaning that in the perturbed system the parameters are assumed to be time-varying [17]. The perturbations need to be small enough to provide "smooth" changes in the parameters; the osculating parameters can be represented by a time-varying state vector $\vec{\boldsymbol{c}} = (a, e, i, \Omega, \omega, \theta)$. The Gaussian Planetary Equations will be a system of 6 intertwined linear equa-

tions that express the evolution of the keplerian parameters over time [17]:

$$\frac{\mathrm{d}\vec{\boldsymbol{c}}}{\mathrm{d}t} = f\left(\vec{\boldsymbol{c}}, t\right)$$

The position and velocity vectors will be expressed as functions of the osculating parameters and time:

$$\begin{aligned} \vec{\boldsymbol{r}} &= \vec{\boldsymbol{x}}\left(\vec{\boldsymbol{c}}, t\right) \\ \vec{\boldsymbol{v}} &= \dot{\vec{\boldsymbol{x}}}\left(\vec{\boldsymbol{c}}, t\right) \end{aligned}$$

The equations of motions, for both the unperturbed and perturbed case, are the following [17]:

$$\begin{aligned} \ddot{\vec{\boldsymbol{x}}}\left(\vec{\boldsymbol{c}}, t\right) + \frac{\mu \vec{\boldsymbol{x}}\left(\vec{\boldsymbol{c}}, t\right)}{\left|\vec{\boldsymbol{x}}\left(\vec{\boldsymbol{c}}, t\right)\right|^3} &= 0 \\ \ddot{\vec{\boldsymbol{x}}}\left(\vec{\boldsymbol{c}}, t\right) + \frac{\mu \vec{\boldsymbol{x}}\left(\vec{\boldsymbol{c}}, t\right)}{\left|\vec{\boldsymbol{x}}\left(\vec{\boldsymbol{c}}, t\right)\right|^3} &= \vec{\boldsymbol{\alpha}} \end{aligned}$$

We can derive the equations to obtain the velocities in both perturbed and unperturbed case [17]:

$$\begin{aligned} \dot{\vec{\boldsymbol{x}}}\left(\vec{\boldsymbol{c}}, t\right) &= \frac{\partial \vec{\boldsymbol{x}}\left(\vec{\boldsymbol{c}}, t\right)}{\partial t} \\ \dot{\vec{\boldsymbol{x}}}\left(\vec{\boldsymbol{c}}, t\right) &= \frac{\partial \vec{\boldsymbol{x}}\left(\vec{\boldsymbol{c}}, t\right)}{\partial t} + \sum_{i=1}^{6} \frac{\partial \vec{\boldsymbol{x}}\left(\vec{\boldsymbol{c}}, t\right)}{\partial c_i} \frac{\mathrm{d}c_i}{\mathrm{d}t} \end{aligned}$$

We want the osculating elements to correspond to the keplerian orbit that has the same state vector both in the perturbed and unperturbed case: this means that the two expressions for the velocity $\dot{\vec{\boldsymbol{x}}}$ must be equal. This translates into the *condition of osculation* [17]:

$$\sum_{i=1}^{6} \frac{\partial \vec{\boldsymbol{x}}\left(\vec{\boldsymbol{c}}, t\right)}{\partial c_i} \frac{\mathrm{d}c_i}{\mathrm{d}t} = 0$$

Deriving again to obtain the acceleration, and applying the condition of osculation, we get [17]:

$$\ddot{\vec{\boldsymbol{x}}}\left(\vec{\boldsymbol{c}}, t\right) = \frac{\partial^2 \vec{\boldsymbol{x}}\left(\vec{\boldsymbol{c}}, t\right)}{\partial t^2} + \sum_{i=1}^{6} \frac{\partial \dot{\vec{\boldsymbol{x}}}\left(\vec{\boldsymbol{c}}, t\right)}{\partial c_i} \frac{\mathrm{d}c_i}{\mathrm{d}t}$$

which inserted into the equation of motion leads to:

$$\frac{\partial^2 \vec{\boldsymbol{x}}\left(\vec{\boldsymbol{c}},t\right)}{\partial t^2}+\sum_{i=1}^{6}\frac{\partial \dot{\vec{\boldsymbol{x}}}\left(\vec{\boldsymbol{c}},t\right)}{\partial c_i}\frac{\mathrm{d}c_i}{\mathrm{d}t}+\frac{\mu \vec{\boldsymbol{x}}\left(\vec{\boldsymbol{c}},t\right)}{\left|\vec{\boldsymbol{x}}\left(\vec{\boldsymbol{c}},t\right)\right|^3}=\vec{\boldsymbol{\alpha}}$$

Now remembering the equation of motion for the unperturbed case, the final expression simplifies to [17]:

$$\sum_{i=1}^{6}\frac{\partial \dot{\vec{\boldsymbol{x}}}\left(\vec{\boldsymbol{c}},t\right)}{\partial c_i}\frac{\mathrm{d}c_i}{\mathrm{d}t}=\vec{\boldsymbol{\alpha}}$$

This last expression provides a system of 3 linear differential equations and is not enough to close the problem for all the 6 parameters. We take now the scalar product of both members and $\partial c_j/\partial \dot{\vec{\boldsymbol{x}}}$ with $j=1,...,6$ to obtain [17]:

$$\sum_{i=1}^{6}\left[\frac{\partial c_j}{\partial \dot{\vec{\boldsymbol{x}}}}\frac{\partial \dot{\vec{\boldsymbol{x}}}}{\partial c_i}\right]\frac{\mathrm{d}c_i}{\mathrm{d}t}=\frac{\partial c_j}{\partial \dot{\vec{\boldsymbol{x}}}}\vec{\boldsymbol{\alpha}}$$

With the 6 keplerian parameters being linearly independent, the term between square brackets [] reduces to the Kronecker function $\delta_{j,i}=1$ for $j=i$ and $\delta_{j,i}=0$ for $j\neq i$. It should be noted that the 6 parameters need not to be the classic keplerian ones, but could be any set of 6 linearly independent parameters that can generate a keplerian orbit. The final equation to calculate the evolution in time of the parameters takes the form [17]:

$$\frac{\mathrm{d}c_j}{\mathrm{d}t}=\frac{\partial c_j}{\partial \dot{\vec{\boldsymbol{x}}}}\vec{\boldsymbol{\alpha}}$$

The derivation for the rate of change of each of the parameters is long and articulated and will not be presented here. Attention should be paid to the fact that each parameter has to be derived with respect to the velocity components, which need to be expressed in the same frame as the acceleration. Detailed derivation can be found in several textbooks such as Vallado's [17]. The form of the equations that will be implemented later in this work is the

following [18]:

$$\begin{aligned}
\frac{\mathrm{d}\Omega}{\mathrm{d}t} &= \frac{r}{p}\frac{\sin(\theta+\omega)}{\sin i}\tilde{\alpha}_z \\
\frac{\mathrm{d}\omega}{\mathrm{d}t} &= -\frac{1}{e}\cos\theta\tilde{\alpha}_x + \left(1+\frac{r}{p}\right)\frac{1}{e}\sin\theta\tilde{\alpha}_y - \frac{r}{p}\cot i\sin(\theta+\omega)\tilde{\alpha}_z \\
\frac{\mathrm{d}i}{\mathrm{d}t} &= \frac{r}{p}\cos(\theta+\omega)\tilde{\alpha}_z \\
\frac{\mathrm{d}a}{\mathrm{d}t} &= \frac{2a^2}{p}\left(e\sin\theta\tilde{\alpha}_x + \frac{p}{r}\tilde{\alpha}_y\right) \\
\frac{\mathrm{d}e}{\mathrm{d}t} &= \sin\theta\tilde{\alpha}_x + \left[\left(1+\frac{r}{p}\right)\cos\theta + e\frac{r}{p}\right]\tilde{\alpha}_y \\
\frac{\mathrm{d}\theta}{\mathrm{d}t} &= \frac{h}{r^2} + \sqrt{\frac{p}{a}}\left[\frac{\cos\theta}{ean}\tilde{\alpha}_x - \left(1+\frac{r}{p}\right)\frac{\sin\theta}{ean}\tilde{\alpha}_y\right]
\end{aligned}$$

In the version of the equations presented above the acceleration terms have been corrected to match the dimensions according to: $(\tilde{\alpha}_x, \tilde{\alpha}_y, \tilde{\alpha}_z) = {}^{h}/_{n^2a^3}(\alpha_x, \alpha_y, \alpha_z)$. To simplify the notation, the semiparameter $p = a(1-e^2)$ has been used, with the obvious assumption that the orbit be elliptic.

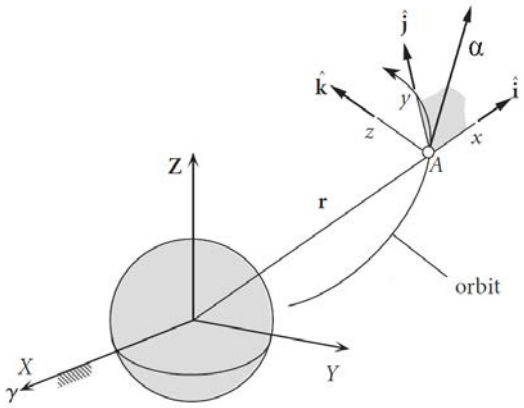

Figure 3.1: Comoving orbital frame of reference [6]

The frame of reference moves with the satellite, with the x axis along the orbital radius and the z axis parallel to the angular moment. The components

of the acceleration in the orbital frame will therefore be:

$$\begin{cases} \alpha_x = \alpha \sin\beta \\ \alpha_y = \alpha \cos\beta \\ \alpha_z = 0 \end{cases}$$

3.1.2 Dimensionless Gaussian Planetary Equations

The equations derived so far can be modified to improve the efficiency of the calculations. Most of the keplerian parameters are dimensionless, others, like the semimajor axis a, are not. The calculations would require several operations between dimensionless parameters, usually close to unit value, and parameters with values that are several orders of magnitude higher than unity (all the parameters that express a length). The best way to approach the integration is by using non-dimensional variables: from now on, plain variables will be intended as dimensionless, while variables with a hat will represent variables with the respective dimensions. The procedure follows from the selection of a scale length a_0 [18]:

- length: $a_0 = L \Longrightarrow \hat{a} = a_0 a$
- time: $\omega_0 = \sqrt{\frac{\mu}{a_0^3}} \Longrightarrow \tau = \omega_0 \hat{t}$
- velocity: $v_0 = a_0\omega_0 \Longrightarrow \hat{v} = v_0 v$
- acceleration: $\alpha_0 = a_0\omega_0^2 \Longrightarrow \hat{\alpha} = \alpha_0\alpha$
- angular moment: $\hat{h} = a_0^2\omega_0 h$

Dimensionless parameters like e and θ will be left unchanged. We introduce the dimensionless parameter χ:

$$\chi = 1 + e\cos\theta = \frac{p}{r}$$

and point out the relation $h = \sqrt{p}$, that can be proved by:

$$\frac{\hat{h}^2}{\mu} = \hat{p} \Longrightarrow \frac{a_0^4\omega_0^2}{\mu}h^2 = a_0 p \Longrightarrow h = \sqrt{p}$$

With these considerations, the non-dimensional GPE assume the form [18]:

$$\begin{aligned}
\frac{\mathrm{d}\Omega}{\mathrm{d}\tau} &= \frac{\sqrt{p}}{\chi}\frac{\sin(\theta+\omega)}{\sin i}\alpha_z \\
\frac{\mathrm{d}\omega}{\mathrm{d}\tau} &= \frac{\sqrt{p}}{e}\left\{-\cos\theta\alpha_x + \left(1+\frac{1}{\chi}\right)\sin\theta\alpha_y - \frac{e}{\chi}\cot i\sin(\theta+\omega)\alpha_z\right\} \\
\frac{\mathrm{d}i}{\mathrm{d}\tau} &= \frac{\sqrt{p}}{\chi}\cos(\theta+\omega)\alpha_z \\
\frac{\mathrm{d}a}{\mathrm{d}\tau} &= \frac{2a^2}{\sqrt{p}}\left\{e\sin\theta\alpha_x + \chi\alpha_y\right\} \\
\frac{\mathrm{d}e}{\mathrm{d}\tau} &= \sqrt{p}\left\{\sin\theta\alpha_x + \left[\left(1+\frac{1}{\chi}\right)\cos\theta + \frac{e}{\chi}\right]\alpha_y\right\} \\
\frac{\mathrm{d}\theta}{\mathrm{d}\tau} &= \frac{\chi^2}{p^{3/2}} + \frac{\sqrt{p}}{e}\left\{\cos\theta\alpha_x - \left(1+\frac{1}{\chi}\right)\sin\theta\alpha_y\right\}
\end{aligned}$$

At this point, a few last steps can be taken to simplify the equation. First of all, in the hypothesis of working with planar orbits, there will be no need to provide an out-of-plane component of the acceleration, which implies $\alpha_z = 0$ eliminating a few of the terms. It can be noticed that both the parameters Ω and i depend entirely on α_z: this means that two equations can be removed from the computation, since the two parameters involved will remain constant. It will prove to be convenient to work with two alternative parameters: the longitude $l = \theta + \omega$ will be substituted to ω and the semiparameter $p = a(1-e^2)$ will be substituted to e. While the derivative of the longitude can be calculated adding the two GPE for θ and ω, the derivative of the semiparameter needs to be calculated through the chain rule:

$$\frac{\mathrm{d}p}{\mathrm{d}\tau} = \frac{\mathrm{d}a}{\mathrm{d}\tau}\left(1-e^2\right) - 2ae\frac{\mathrm{d}e}{\mathrm{d}\tau}$$

For each step of the integration the eccentricity can be derived from a and p: $e = \sqrt{1 - {}^{p}/_{a}}$. We finally get to the final form of the 4 GPE that will be

used for the integration of the equations of motion [18]:

$$\begin{aligned}
\frac{\mathrm{d}a}{\mathrm{d}\tau} &= \frac{2a^2}{\sqrt{p}}\left\{e\sin\theta\alpha_x + \chi\alpha_y\right\} \\
\frac{\mathrm{d}p}{\mathrm{d}\tau} &= 2\frac{p^{3/2}}{\chi}\alpha_y \\
\frac{\mathrm{d}\theta}{\mathrm{d}\tau} &= \frac{\chi^2}{p^{3/2}} + \frac{\sqrt{p}}{e}\left\{\cos\theta\alpha_x - \left(1+\frac{1}{\chi}\right)\sin\theta\alpha_y\right\} \\
\frac{\mathrm{d}l}{\mathrm{d}\tau} &= \frac{\chi^2}{p^{3/2}}
\end{aligned}$$

3.2 Low Thrust equations

In this chapter we will analyze different aspects of the low-thrust theory. As mentioned previously, the aim of applying a low-thrust arc is to reduce the relative velocity between the spacecraft and the target planet, in our case Saturn. In order to do so, the thrust needs to be pointing along an optimal direction to provide the desired variation in the parameters of the spacecraft's orbit. Assuming that we want to reach Saturn in a specific position, the optimal solution to reduce the v_∞ is to have the spacecraft put onto an orbit that is tangent to Saturn's at the intersection point. To minimize the v_∞, the parameters of the transfer orbit need to approach those of Saturn's orbit, with the upper bound of $v_\infty = 0$ when the satellite is inserted into Saturn's orbit. In the following sections, the subscript 'S' will indicate parameters of Saturn's orbit, while the subscript 'f' will refer to the spacecraft's parameters after the thrust arc.

3.2.1 Circular Orbit approximation

Initially we will make the assumption of Jupiter's and Saturn's orbit being circular. The real position of the planets will also be neglected for the time being, as the main focus is to identify how to perform the thrust arc to

optimize the capture. The purpose is to reach an altitude equal to Saturn's radius that is, in this case, a_S; when in the intersection point we have:

$$a_S = \frac{a_f(1-e_f^2)}{1+e_f\cos\theta_f} = \frac{p_f}{1+e_f\cos\theta_f}$$

from which we can easily calculate:

$$\cos\theta_f = \frac{1}{e_f}\left(\frac{p_f}{a_S} - 1\right)$$

In the two equations above, θ_f is the true anomaly of the S/C at the intersection point with Saturn. We can discriminate between three cases:

- $|\cos\theta_f| < 1$: the spacecraft intersects Saturn's orbit;
- $|\cos\theta_f| = 1$: the spacecraft's orbit is tangent to Saturn's orbit at it's apoapse;
- $|\cos\theta_f| > 1$: the spacecraft does not intersect Saturn's orbit.

Notable Equations and Parametrization

- Tangency condition: the Γ curve
  Let's consider transfer orbits that are tangent to Saturn's orbit. In this circumstance $\cos\theta_f = -1$ so we obtain [18]:

$$\begin{cases} a_S = a_f(1+e_f) \\ p_f = a_f(1-e_f^2) \end{cases}$$

  In our analysis, the variables of the optimization will be a_f and p_f, while e_f can be calculated from the other two. The two variables will be better expressed through the additional following parametrization [18]:

$$\xi = \frac{a_f}{a_S} \qquad\qquad \eta = \frac{p_f}{a_S}$$

Eliminating the parameter e from the equations above and substituting the new variables leads to the formulation of the Γ curve [18]:

$$\Gamma : 2 - \frac{1}{\xi} - \eta = 0$$

In the (ξ, η) plane this curve is the locus of points that correspond to an orbit that has its apogee on Saturn's orbit; all the points below the curve correspond to orbits that intersect Saturn's orbit, while those lying above correspond to orbits that do not [18].

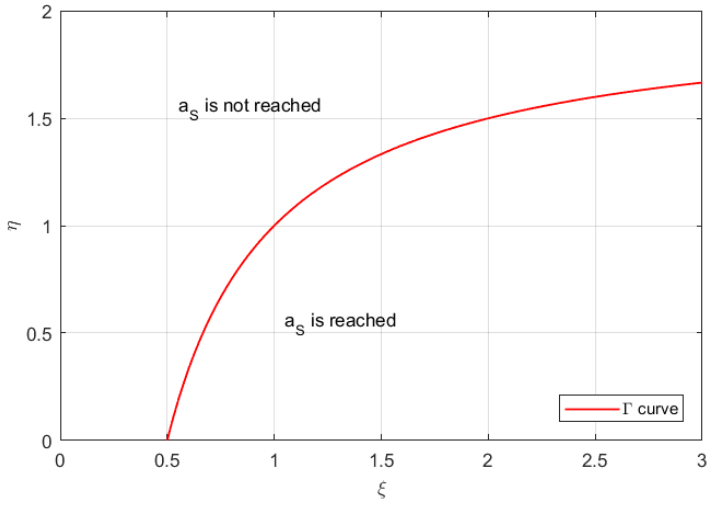

Figure 3.2: Γ curve [18]

- Relative Velocity: the σ parameter

  When the final orbit reaches Saturn, meaning the two orbits do intersect, we can calculate the relative velocity v_∞ at the intersection point. The velocities of both planet and S/C can be expressed in polar

coordinates:

$$\begin{aligned}\vec{\boldsymbol{v}}_f &= \left\{\frac{1}{\sqrt{p_f}} e_f \sin\theta_f\right\}\hat{\boldsymbol{u}}_r + \left\{\frac{1}{\sqrt{p_f}}\left(1+e_f\cos\theta_f\right)\right\}\hat{\boldsymbol{u}}_\theta \\ \vec{\boldsymbol{v}}_S &= \left\{\frac{1}{\sqrt{a_S}}\right\}\hat{\boldsymbol{u}}_\theta\end{aligned}$$

and the module of v_∞ needs to be calculated vectorially [18]:

$$\begin{aligned}v_\infty^2 &= \left(\frac{1}{\sqrt{p_f}} e_f \sin\theta_f\right)^2 + \left(\frac{1}{\sqrt{p_f}}\left(1+e_f\cos\theta_f\right) - \frac{1}{\sqrt{a_S}}\right)^2 \\ &= -\frac{1-e_f^2}{p_f} + 2\frac{1+e_f\cos\theta_f}{p_f} + \frac{1}{a_S} - 2\frac{1+e_f\cos\theta_f}{p_f}\sqrt{\frac{p_f}{a_S}} \\ &= \frac{3}{a_S} - \frac{1}{a_f} - 2\sqrt{\frac{p_f}{a_S^3}}\end{aligned}$$

Defining the new parameter $\sigma = a_s v_\infty^2$ and adopting the same variables (ξ, η) introduced in the previous chapters, leads to [18]:

$$\sigma = 3 - \frac{1}{\xi} - 2\sqrt{\eta}$$

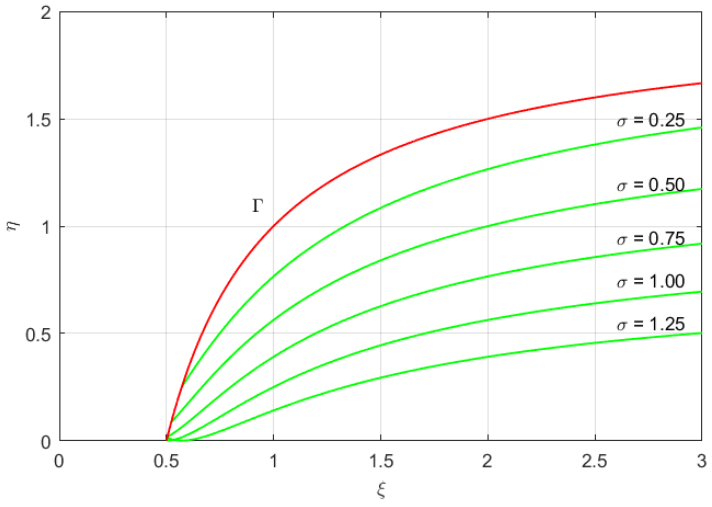

Figure 3.3: Curves at constant values of σ [18]

For a given σ, the intersection point between the curve at constant σ and the Γ curve provides the semimajor axis and semiparameter of the orbit, tangent to Saturn's orbit, whose relative velocity corresponds to σ. In such a case, with Saturn's velocity being higher than the spacecraft's, we have [18]:

$$\begin{aligned} v_\infty &= \frac{1}{\sqrt{a_S}} - \frac{1}{\sqrt{p_f}}(1 - e_f) \\ \sqrt{\sigma} &= 1 - \frac{1 - e_f}{\sqrt{\eta}} \end{aligned}$$

From this last equation we remind that we have [18]:

$$a_f(1 - e_f^2) = a_S \Longrightarrow e_f = \frac{1}{\chi} - 1$$

and from the equation of the Γ curve [18]:

$$2 - \frac{1}{\xi} = \eta$$

which lead to:

$$\sqrt{\sigma} = 1 - \sqrt{\eta}$$

This last equation explains that, in order to minimize σ, which is the relative velocity, we need to maximize the semiparameter η.

- <u>The transfer orbit does not reach Saturn</u>
  If the transfer orbit does not reach Saturn's orbit, it means the apoapse lies at a lower altitude than a_S; in this case, the relative velocity v_∞ is defined as the difference between the spacecraft's velocity at its apoapse and Saturn's velocity when it lies on the radial direction that joins the Sun with the S/C [18]. When Saturn and the spacecraft have different phases, the relative velocity is higher. Again we have:

$$v_\infty = \frac{1}{\sqrt{a_S}} - \frac{1}{\sqrt{p_f}}(1 - e_f)$$

A similar analysis to that in the previous section leads to [18]:

$$\begin{aligned} \sqrt{\sigma} &= 1 - \frac{\sqrt{\eta}}{\xi + \sqrt{\xi\,(\xi - \eta)}} \\ \eta &= \left\{ \frac{1}{2\xi\,(1 - \sqrt{\sigma})} + \frac{1}{2}\left(1 - \sqrt{\sigma}\right) \right\}^{-2} \end{aligned}$$

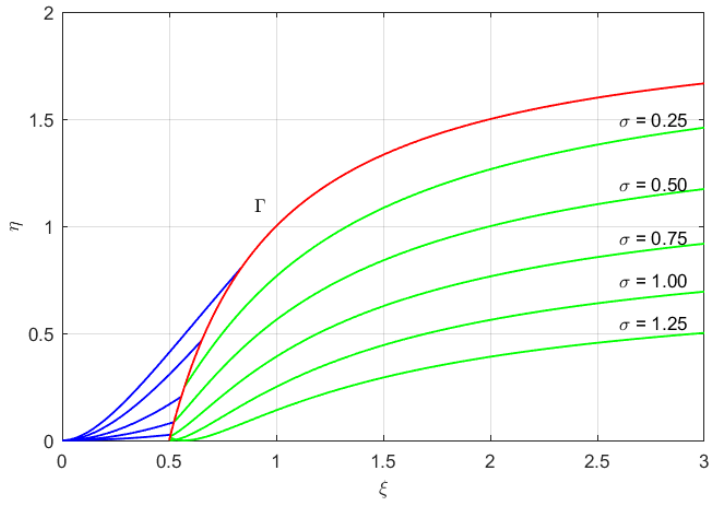

Figure 3.4: Curves at constant values of σ; those which reach Saturn in green and those who do not in blue [18]

Optimal Control Laws

The purpose of this section is to identify the most efficient way to apply the thrust arc in order to produce the desired variations in the orbital parameters. Three main techniques will be investigated, which apply to different circumstances that may characterize the unpropelled transfer orbit; as we will see in future sections, combination of multiple control strategies are also feasible.

- The transfer orbit intersects Saturn's orbit
  In this case, the best control strategy is to decrease σ until the tangency

condition is reached. The most efficient way to do so is by moving in the (ξ, η) plane perpendicularly to the curves at constant σ [18]. The gradient of a curve at constant σ provides the perpendicular direction:

$$\vec{\boldsymbol{n}} = \vec{\nabla}\boldsymbol{\sigma} = \left(\frac{\partial\sigma}{\partial\xi}, \frac{\partial\sigma}{\partial\eta}\right) = \left(\frac{1}{\xi^2}, -\frac{1}{\sqrt{\eta}}\right)$$

This provides restrictions for the time-evolution of the variables [18]:

$$\begin{cases} \dfrac{\mathrm{d}\xi}{\mathrm{d}\tau} = \lambda\dfrac{1}{\xi^2} \\ \dfrac{\mathrm{d}\eta}{\mathrm{d}\tau} = -\lambda\dfrac{1}{\sqrt{\eta}} \end{cases} \implies \frac{\mathrm{d}\xi}{\mathrm{d}\tau}\frac{1}{\sqrt{\eta}} + \frac{\mathrm{d}\eta}{\mathrm{d}\tau}\frac{1}{\xi^2} = 0$$

Remembering the dimensionless GPE's and that (ξ, η) are proportional to (a, p) leads to [18]:

$$\frac{\mathrm{d}a}{\mathrm{d}\tau}\sqrt{\frac{a_S}{p}} + \frac{\mathrm{d}p}{\mathrm{d}\tau}\frac{a_s^2}{a^2} = 0$$

Substituting the equations for the time derivatives and the decomposition for the acceleration vector we obtain [18]:

$$t_c \sin\beta + t_s \cos\beta = 0$$

where:

$$\begin{cases} t_c = e\sin\theta \\ t_s = \chi + \dfrac{a_S^{3/2}p^{5/2}}{\chi a^4} \end{cases} \iff \begin{cases} t_c = e\sin\theta \\ t_s = \chi + \dfrac{\eta^{5/2}}{\chi\xi^4} \end{cases}$$

The optimal value for β is therefore [18]:

$$\begin{cases} \sin\beta = \Lambda t_s \\ \cos\beta = \Lambda t_c \end{cases} \implies \beta = \arctan 2(\Lambda t_s, -\Lambda t_c)$$

The absolute value of Λ can be any real number different from 0, so we assume $|\Lambda| = 1$. The sign of Λ, however, needs to be chosen in order to increase the semiparameter p [18]:

$$\frac{\mathrm{d}p}{\mathrm{d}\tau} = -\left[2\frac{p^{3/2}}{\chi}e\alpha\right]\Lambda\sin\theta > 0$$

Therefore we choose Λ to have the opposite sign of $\sin\theta$ [18].

- The transfer orbit is tangent to Saturn's orbit

  When the transfer orbit already is tangent to Saturn's orbit, it means it represents a point that lies on the Γ curve: the best way to proceed is to reduce σ moving the parameters of the S/C along the Γ curve. The perpendicular direction to the curve is [18]:

  $$\vec{\boldsymbol{n}} = \vec{\nabla}\boldsymbol{\Gamma} = \left(\frac{\partial\Gamma}{\partial\xi}, \frac{\partial\Gamma}{\partial\eta}\right) = \left(\frac{1}{\xi^2}, -1\right)$$

  To move along the curve, we want the vector

  $$\vec{\boldsymbol{t}} = \left(\frac{\mathrm{d}\xi}{\mathrm{d}\tau}, \frac{\mathrm{d}\eta}{\mathrm{d}\tau}\right)$$

  to be perpendicular to $\vec{\boldsymbol{n}}$. This leads to [18]:

  $$\frac{\mathrm{d}\xi}{\mathrm{d}\tau}\frac{1}{\xi^2} - \frac{\mathrm{d}\eta}{\mathrm{d}\tau} = 0$$

  Similarly to what was done in the previous case, this leads to [18]:

  $$t_c \sin\beta + t_s \cos\beta = 0$$

  where:

  $$\begin{cases} t_c = e\sin\theta \\ t_s = \chi + \dfrac{\eta^2}{\chi} \end{cases} \Longrightarrow \beta = \arctan 2(\Lambda t_s, -\Lambda t_c)$$

  Again, we choose the absolute value of Λ in order to increase p:

  $$\frac{\mathrm{d}p}{\mathrm{d}\tau} = -\left[2\frac{p^{3/2}}{\chi}e\alpha\right]\Lambda\sin\theta > 0$$

  Therefore we choose Λ to have the opposite sign of $\sin\theta$ [18].

- The transfer orbit does not intersect Saturn's orbit

  When the transfer orbit does not intersect Saturn's orbit, the thrust must be provided in order to raise the apoapse to Saturn's altitude. Let in this case be [18]:

  $$\vec{\boldsymbol{n}} = \vec{\nabla}\sqrt{\boldsymbol{\sigma}} = \left(\frac{\partial\sqrt{\sigma}}{\partial\xi}, \frac{\partial\sqrt{\sigma}}{\partial\eta}\right) = (n_\xi, n_\eta)$$

And the equation that allow to reach the Γ curve moving along a curve at constant σ is [18]:

$$\frac{\mathrm{d}\xi}{\mathrm{d}\tau}n_\xi + \frac{\mathrm{d}\eta}{\mathrm{d}\tau}n_\eta = 0$$

Similarly to what was done in the previous cases, this leads to [18]:

$$t_c \sin\beta + t_s \cos\beta = 0$$

where:

$$\begin{cases} t_c = e\chi \sin\theta \\ t_s = \chi^2 - \dfrac{\eta}{\sqrt{\xi}(\sqrt{\xi} + \sqrt{\xi - \eta})} \end{cases} \implies \beta = \arctan 2(\Lambda t_s, -\Lambda t_c)$$

Again, we choose the absolute value of Λ in order to increase p:

$$\frac{\mathrm{d}p}{\mathrm{d}\tau} = -\left[2p^{3/2}e\alpha\right]\Lambda \sin\theta > 0$$

Therefore we choose Λ to have the opposite sign of $\sin\theta$ [18].

3.2.2 Elliptic orbits

In this section we will see how the equations developed in the previous sections can be extended and adapted for a problem that aims at intersecting a target planet that lies on an elliptic orbit. The concepts and purpose are the same as before, but a degree of approximation is removed in order to provide more accurate results in the perspective of a future application of the theory. The theory revolves around the assumption of optimizing the equations for the real intersection point between the transfer orbit and Saturn's orbit. The subscripts used will be the same as those used previously, referring to the keplerian parameters after the thrust arc; the angles θ_S and θ_f will refer to the true anomalies of Saturn and the transfer orbit respectively, at the intersection point r.

$$r = \frac{a_S(1-e_S^2)}{1+e_S\cos\theta_S} = \frac{a_f(1-e_f^2)}{1+e_f\cos\theta_f} = \frac{p_S}{1+e_S\cos\theta_S} = \frac{p_f}{1+e_f\cos\theta_f}$$

Notable Equations and Parametrization

- Relative Velocity: the σ parameter

  The velocities of both Saturn and the S/C are expressed in polar coordinates, only in this case the radial component of Saturn's velocity will not be neglected:

$$\begin{aligned}\vec{\boldsymbol{v}}_f &= \left\{\frac{1}{\sqrt{p_f}} e_f \sin\theta_f\right\}\hat{\boldsymbol{u}}_r + \left\{\frac{1}{\sqrt{p_f}}\left(1+e_f\cos\theta_f\right)\right\}\hat{\boldsymbol{u}}_\theta \\ \vec{\boldsymbol{v}}_S &= \left\{\frac{1}{\sqrt{p_S}} e_S \sin\theta_S\right\}\hat{\boldsymbol{u}}_r + \left\{\frac{1}{\sqrt{p_S}}\left(1+e_S\cos\theta_S\right)\right\}\hat{\boldsymbol{u}}_\theta\end{aligned}$$

  and the module of v_∞ needs to be calculated vectorially:

$$\begin{aligned}v_\infty^2 =& \left(\frac{1+e_f\cos\theta_f}{\sqrt{p_f}} - \frac{1+e_S\cos\theta_S}{\sqrt{p_S}}\right)^2 + \left(\frac{e_f\sin\theta_f}{\sqrt{p_f}} - \frac{e_S\sin\theta_S}{\sqrt{p_S}}\right)^2 \\ =& \frac{1+e_f^2+2e_f\cos\theta_f}{p_f} + \frac{1+e_S^2+2e_S\cos\theta_S}{p_S} + \\ & - \frac{2}{\sqrt{p_f p_S}}\left[(1+e_f\cos\theta_f)(1+e_S\cos\theta_S) + e_f e_S \sin\theta_f\sin\theta_S\right] \\ =& \frac{4}{r} - \frac{1}{a_f} - \frac{1}{a_S} - \frac{2}{r}\sqrt{\frac{p_f p_S}{r^2}} - 2\left[\frac{e_f\sin\theta_f}{\sqrt{p_f}}\frac{e_S\sin\theta_S}{\sqrt{p_S}}\right]\end{aligned}$$

  At this point the term between square brackets [] needs to be manipulated a bit. Let's remind that the radial velocity of an orbiting body is expressed by the equation:

$$v_{r,i} = \frac{e_i\sin\theta_i}{\sqrt{p_i}}$$

  We now take the equation of the orbital energy for an elliptic orbit, in its dimensionless form, and divide it by the semiparameter p:

$$\frac{v_r^2+v_\theta^2}{2p} - \frac{1}{pr} = -\frac{1}{2pa}$$

$$\frac{v_r^2}{p} = \frac{2}{pr} - \frac{1}{pa} - \frac{v_\theta^2}{p}$$

and remind that the following relation holds for the normal component of the velocity:

$$\frac{v_\theta^2}{p} = \frac{1}{p}\left(\frac{1+e\cos\theta}{\sqrt{p}}\right)^2 = \frac{1}{r^2}$$

which substituted into the last equation leads to the expression:

$$v_r = \pm\sqrt{\frac{2}{r} - \frac{1}{a} - \frac{p}{r^2}}$$

where the $\pm$ sign is chosen according to whether the radial velocity v_r is directed outwards ($\theta \in [0, \pi]$) or inwards ($\theta \in [\pi, 2\pi]$). This equation for v_r can be substituted into the last expression for the hyperbolic excess velocity giving:

$$v_\infty^2 = \frac{4}{r} - \frac{1}{a_f} - \frac{1}{a_S} - \frac{2}{r}\sqrt{\frac{p_f p_S}{r^2}} \mp 2\sqrt{\frac{2}{r} - \frac{1}{a_f} - \frac{p_f}{r^2}}\sqrt{\frac{2}{r} - \frac{1}{a_S} - \frac{p_S}{r^2}}$$

At this point we adopt a parametrization similar to that of section 3.2.1, for both transfer orbit and Saturn's orbit:

$$\begin{cases} \xi = \dfrac{a_f}{r} \\ \eta = \dfrac{p_f}{r} \end{cases} \qquad\qquad \begin{cases} \phi = \dfrac{a_S}{r} \\ \psi = \dfrac{p_S}{r} \end{cases}$$

which lead to the final expression for σ:

$$\sigma = r v_\infty^2 = 4 - \frac{1}{\phi} - \frac{1}{\xi} - 2\sqrt{\psi\eta} \mp 2\sqrt{2 - \frac{1}{\phi} - \psi}\sqrt{2 - \frac{1}{\xi} - \eta}$$

It is easy to verify that with the approximation of Saturn's orbit being circular ($a_S = p_S = r$) the last equation leads back to the original formulation:

$$\sigma = a_S v_\infty^2 = 3 - \frac{1}{\xi} - 2\sqrt{\eta}$$

- Tangency condition: the Γ curve

  In the (ξ, η) plane, the Γ curve is the locus of points that correspond to

the orbits that are tangent to Saturn's orbit at the given intersection point. Considering the orbit as elliptic, the tangency is granted when the local velocity of the planet and that of the satellite are parallel. Equivalently, the cross product of the two velocity vectors has to be equal to zero. Since the orbits are planar, it will suffice to calculate the out-of-plane component of said cross product and equate it to zero:

$$v_{rf}v_{\theta S} - v_{rS}v_{\theta f} = 0$$

We now multiply both terms by $\frac{1}{\sqrt{p_f p_S}}$ and remembering that $\frac{v_{\theta i}}{\sqrt{p_i}} = \frac{1}{r}$ leads to:

$$\frac{1}{r}\left(\frac{v_{rf}}{\sqrt{p_f}} - \frac{v_{rS}}{\sqrt{p_S}}\right) = 0$$

With the same substitution applied before, squaring the two terms of the equation leads to:

$$\Gamma_{\phi,\psi} : \frac{1}{\phi} + \psi - \frac{1}{\xi} - \eta = 0$$

Again, in case of circular orbit the last equation falls back into the case:

$$\Gamma_{\phi,\psi} : 2 - \frac{1}{\xi} - \eta = 0$$

Attention needs to be paid to the fact that the $\Gamma_{\phi,\psi}$ curve depends on the position of the intersection point, through the parameter r. The shape of the curve, in fact, will change slightly according to the real position of the target planet on its elliptical orbit.

Optimal Control Laws

Assuming that, after performing a flyby around Jupiter, the transfer orbit intersects Saturn's orbit, we want to provide a version of the optimal control equations presented earlier but applied to the case of an elliptic target orbit.

- Reaching tangency condition

  Again we want to move in the (ξ, η) plane perpendicularly to the curves at constant σ. The gradient of a curve at constant σ in this case is:

$$\vec{\boldsymbol{n}} = \vec{\nabla}\boldsymbol{\sigma} = \left(\frac{\partial\sigma}{\partial\xi}, \frac{\partial\sigma}{\partial\eta}\right) = \left(\frac{1}{\xi^2}(1 \mp H), -\sqrt{\frac{\psi}{\eta}} \pm H\right)^{3}$$

  where:

$$H = \sqrt{\frac{2 - 1/\phi - \psi}{2 - 1/\xi - \eta}}$$

  And from analogous considerations to the circular orbit case, the equation for the optimal control is:

$$\frac{\mathrm{d}\xi}{\mathrm{d}\tau}\frac{\partial\sigma}{\partial\eta} - \frac{\mathrm{d}\eta}{\mathrm{d}\tau}\frac{\partial\sigma}{\partial\xi} = 0$$

  Which leads to:

$$t_c \sin\beta + t_s \cos\beta = 0$$

  where:

$$\begin{cases} t_c = & e\sin\theta \\ t_s = & \chi + \dfrac{\eta^2}{\chi\xi^4}\dfrac{1 \mp H}{\sqrt{\psi/\eta} \mp H} \end{cases}^{3}$$

  The optimal value for β is therefore:

$$\begin{cases} \sin\beta = \Lambda t_s \\ \cos\beta = \Lambda t_c \end{cases} \Longrightarrow \beta = \arctan 2(\Lambda t_s, -\Lambda t_c)$$

  with the identical considerations about Λ.

[3]The $(\mp)$ sign varies according to the orientations of radial velocities v_{rS} and v_{rf} : when $\sin\theta_f \sin\theta_S > 0$, the $(\mp)$ becomes a minus (-), when $\sin\theta_f \sin\theta_S < 0$, becomes a plus (+).

- Maintaining tangency condition

  The control law for moving along the $\Gamma_{\phi,\psi}$ curve is identical to the one for the circular approximation case:

$$\vec{\boldsymbol{n}} = \vec{\nabla}\boldsymbol{\Gamma_{\phi,\psi}} = \left(\frac{\partial\Gamma_{\phi,\psi}}{\partial\xi}, \frac{\partial\Gamma_{\phi,\psi}}{\partial\eta}\right) = \left(\frac{1}{\xi^2}, -1\right)$$

  which also leads to:

$$\begin{cases} t_c = e\sin\theta \\ t_s = \chi + \dfrac{\eta^2}{\chi} \end{cases} \Longrightarrow \beta = \arctan 2(\Lambda t_s, -\Lambda t_c)$$

  With the usual considerations about Λ.

Chapter 4

Implementation and Results

4.1 General concepts

In this chapter we will develop the results obtained in section 2.3 applying the theory laid out in chapter 3 for an elliptic target orbit. The orbital design considered will be the second one presented, involving a free flyby around Jupiter; the parameter chosen as scale length is the heliocentric radius of the intersection point between Saturn and the transfer orbit: $a_0 = \hat{r}$. This choice proves to be efficient because it reduces all the length quantities to values lower than 1, and with $r = 1$ the parameters (ξ, η) and (ϕ, ψ) result numerically equal to the dimensionless values of (a_f, p_f) and (a_S, p_S) respectively, avoiding additional manipulation for the parameters involved in the optimal control. The Gaussian Planetary Equations will be solved using MATLAB®/ Simulink implementing the Runge-Kutta(4,5) method (ode45). In the simulation, the thrust appears in the form of a square wave with amplitude equal to the acceleration in the time interval while the thruster is on, and equal to zero when turned off; the simulation terminates when the orbital radius of the transfer orbit reaches $r = 1$. The dimensionless parameters of the transfer orbit are reported in table 4.1. As mentioned previously, there are four main design drivers in the process of optimizing

Transfer orbit 2			
e	0.455335	a	0.6873765
i	0.0	$\theta_{departure}$ (rad)	1.546061
ω (deg)	88.6728	$\theta_{arrival}$ (rad)	3.112125
Ω	/	ΔT	1.365526

Table 4.1: Dimensionless parameters of the Jupiter-to-Saturn transfer orbit

the trajectory: the thrust direction angle β, the acceleration provided by the thruster α, the time during which the thruster is turned on T_{thr} and the time to be waited, from the departure from Jupiter, before turning on the thruster δ. As seen in chapter 3, the angle β can be derived from the most suitable optimal control laws, and is therefore defined in every circumstance. As can be seen from the control laws for β, the angle is independent from the acceleration provided: intuitively, this means that the acceleration does not affect the path that joins different points along the Γ planecurve, but only the time it requires the thruster to cover that path. In each of the analyses presented the angle β was calculated in order to reach tangency condition firs, at to move along the Γ curve subsequently. An example of the evolution of the transfer orbit in the (ξ, η) plane is presented in fig. 4.1.

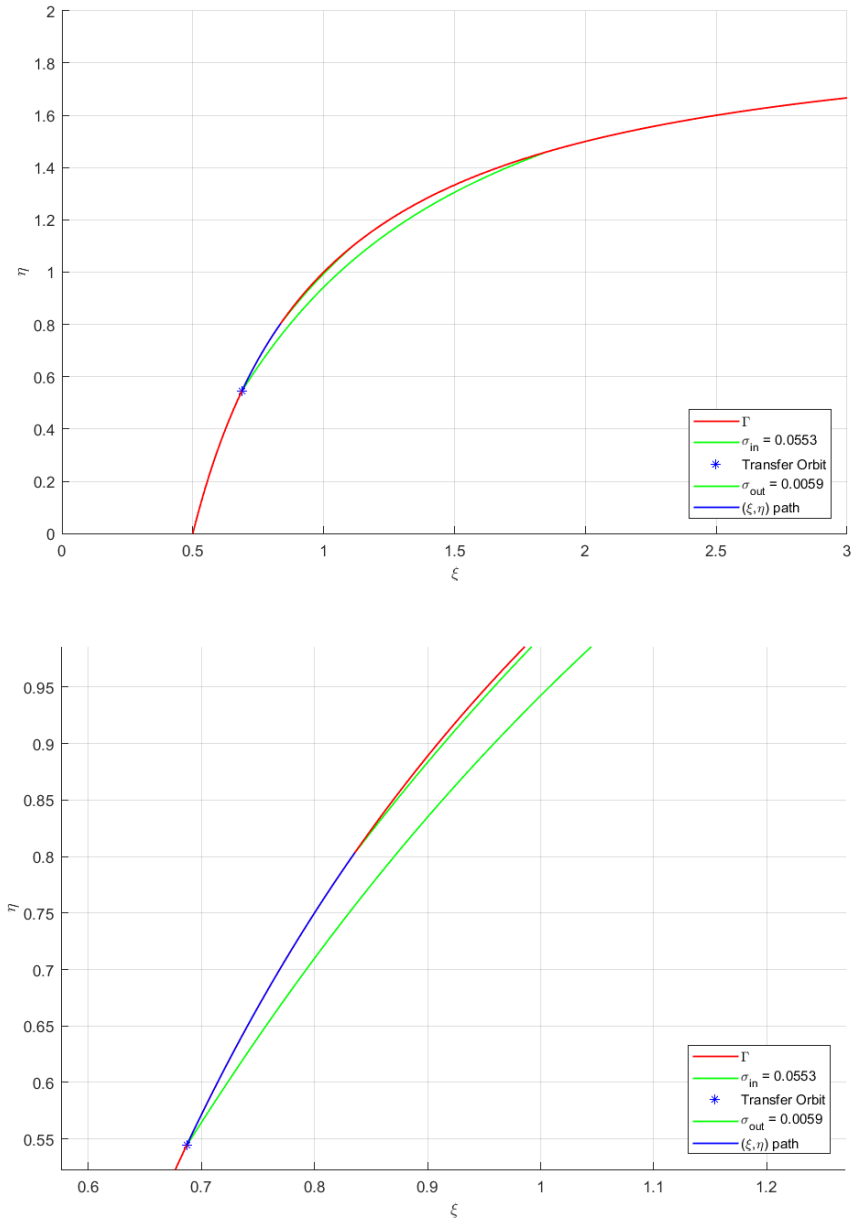

Figure 4.1: Evolution along the (ξ, η) plane with $\alpha = 0.3$ and $T_{thr} = 5$ years

4.2 Optimal choices for α, T_{thr} and δ

Several simulations were run with a variety of values for each parameter: the purpose is to identify significant correlations among the parameters and optimal values for the implementation of the method that are not evident from a first mathematical analysis. The test values for the acceleration are $\alpha \in [0.2, 0.4]$ which correspond, for a spacecraft with a mass of 1000 kg, to a thrust that falls in the range $F \in [10, 25]$ mN; these values were chosen based on the performances of a variety of ion thrusters and hall effect thrusters currently available on the market [19] so that the thruster's power requirement would not exceed the indicative value of 400 W, which can be provided through RTG's. The values for T_{thr} correspond to several years of activity, as electric thrusters usually have a life expectancy of above 2 years [20, 21]. Hypothetically, should a thruster require a T_{thr} longer than its own expected lifetime, more thrusters can be utilized in sequence to provide thrust when the firs one(s) cease to function, as electric thrusters have a very low impact on the mass budget of the mission.

4.2.1 Simulations with constant T_{thr}

In this first subcase, several simulations were run assuming a constant value for $T_{thr} = 2.5$ years. The independent variable in the plots is the delay time δ; curves are given for different values of α.
As can be noted from the graphs, a higher acceleration (meaning a higher thrust) results in a much lower relative speed at the encounter. As a downside, a higher thrust implies a higher total flight time, as it can be visualized in fig. 4.2. There is an optimal choice for the delay time δ: looking simultaneously at fig. 4.2 and 4.3, it can be noted that the minimum relative velocity for each curve is reached when the thruster is turned on exactly 2.5 years before the end of the total fight time. This means that the optimal position for the thrust arc is at the exact end of the transfer orbit.

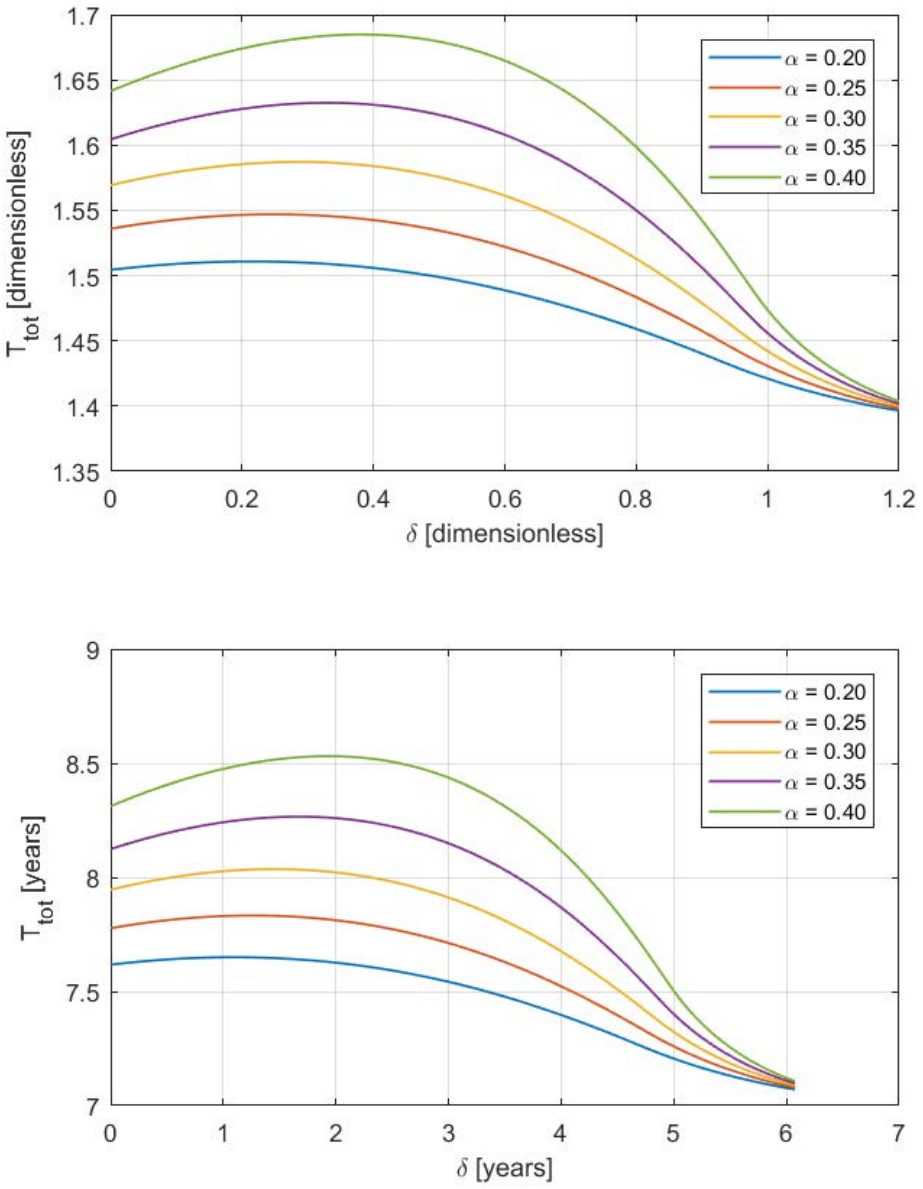

Figure 4.2: Total time of flight for different values of δ and α

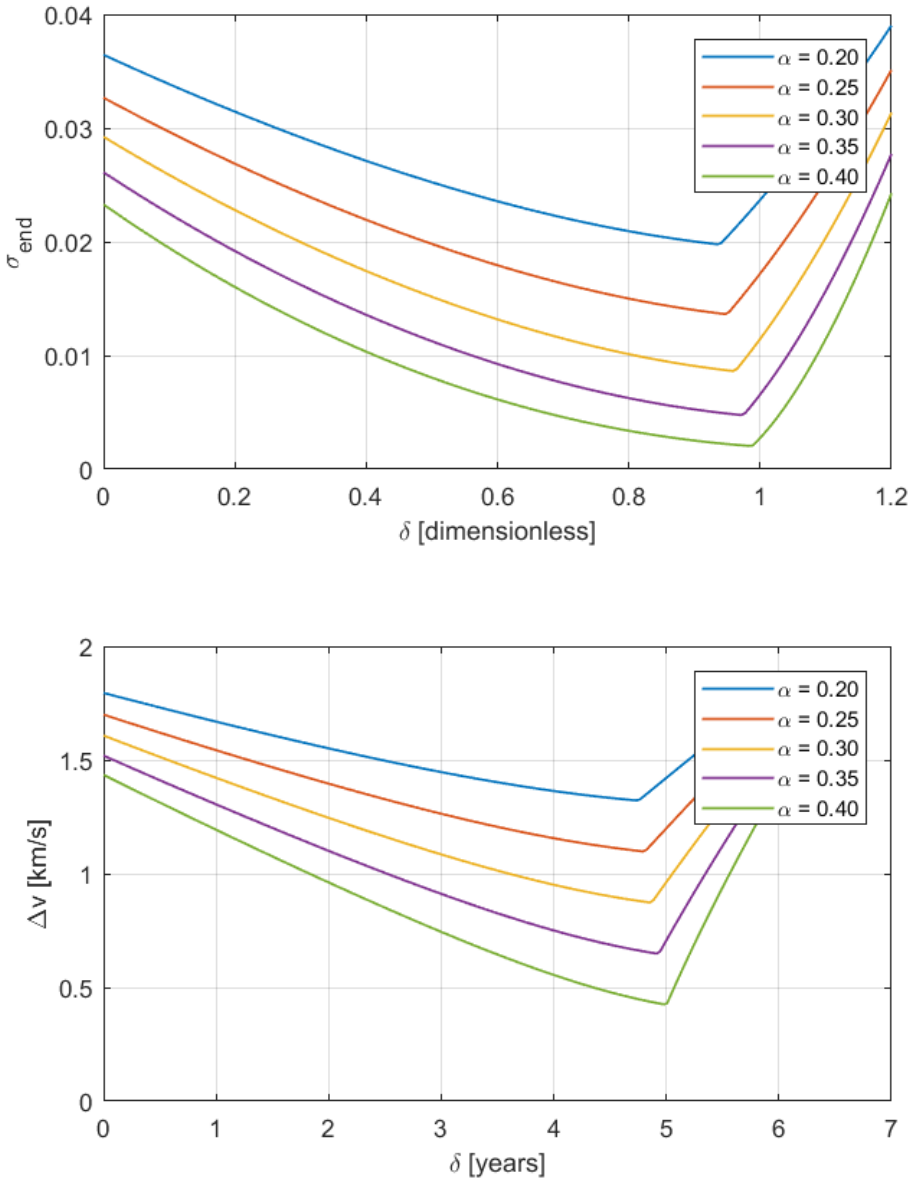

Figure 4.3: v_∞ for different values of δ and α

4.2.2 Simulations with constant α

In this second simulation, the acceleration parameter has been kept constant to $\alpha = 0.3$, while the time of thrust is the parameter that changes in the different curves. Again the independent variable is the delay time δ.
In this case as well, the behavior of the curves is qualitatively similar: increasing T_{thr} allows to reduce the v_∞, at the expenses of a higher total flight time, as can be seen in fig. 4.4. Once more, comparing fig. 4.4 and 4.5 the optimal value for the delay δ appears to be the one consisting in placing the thrust arc at the exact end of the transfer orbit. One interesting observation about these last charts is the fact that for sufficiently high values of δ the curves at different T_{thr} overlap: this makes sense because when the thruster is turned on, for example, 2.5 years before reaching Saturn's altitude, the integration is not affected by how long the thruster can keep working, and will stop once the condition $r = 1$ is reached, regardless of how long the thruster could hypothetically keep working.

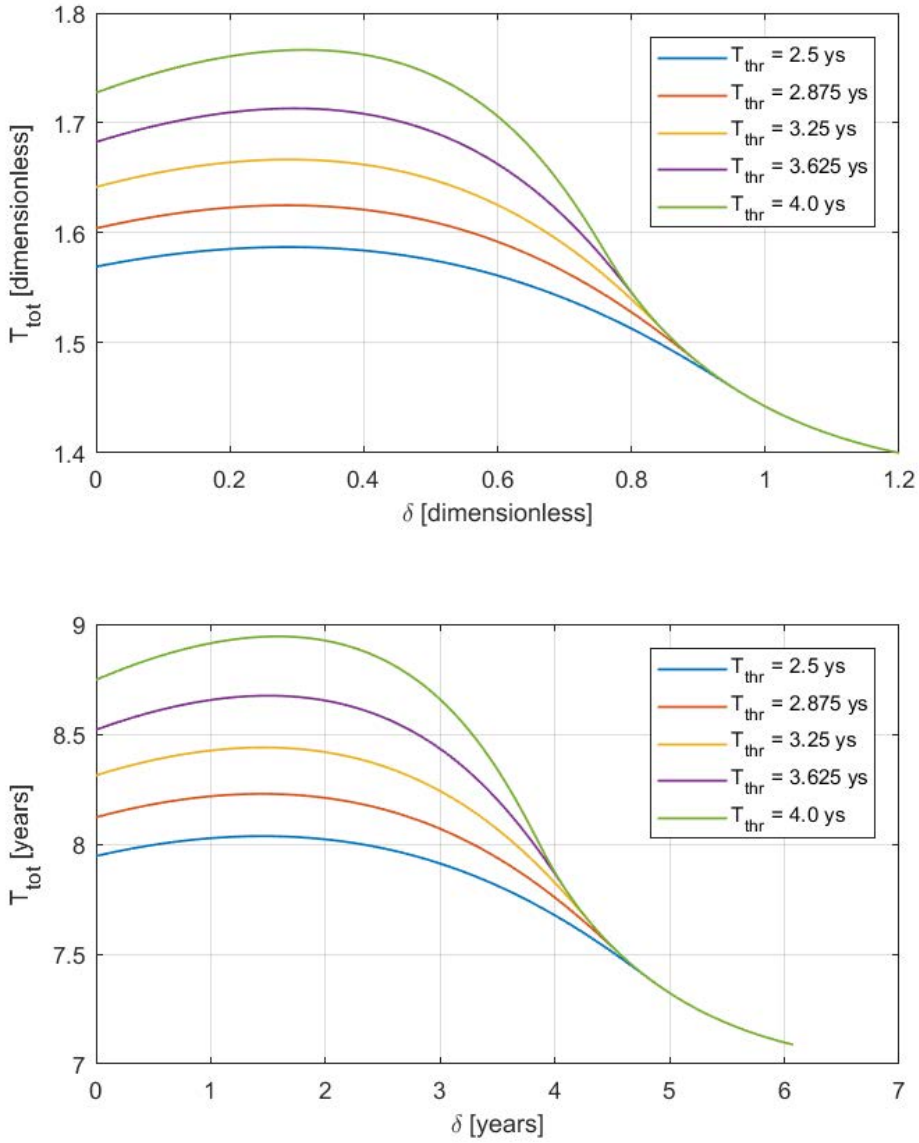

Figure 4.4: Total time of flight for different values of δ and T_{thr}

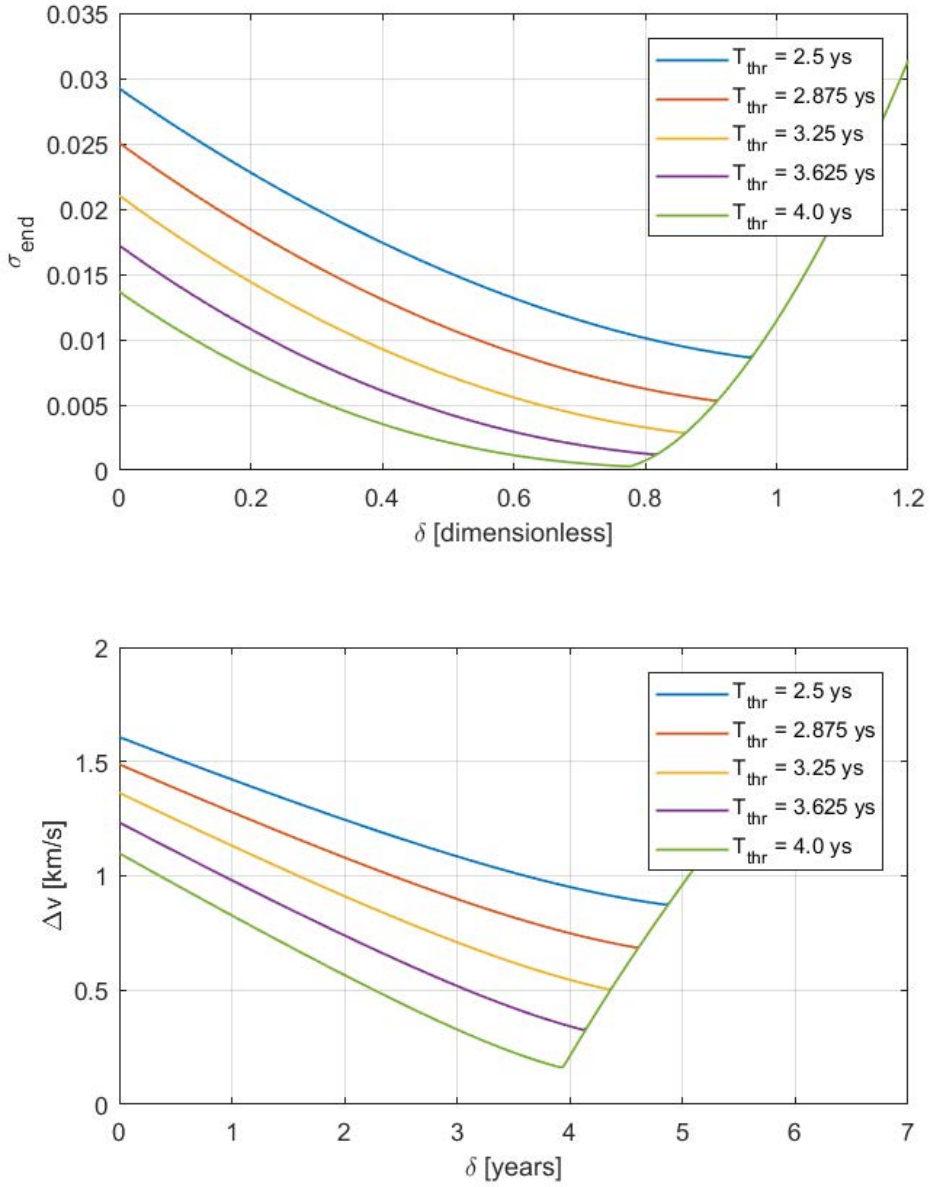

Figure 4.5: v_∞ for different values of δ and T_{thr}

4.2.3 Simulations with optimal δ values

It appears clear that the optimal location of the thrust arc is at the end of the transfer orbit, regardless of the other parameters involved. The degree of freedom of δ is here removed as, for each combination of parameters, the δ value is chosen in order to provide the minimum v_∞ of each curve. The curves provide the relative velocity v_∞ as function of the thrust time, for different values of the acceleration, and can be visualized in fig. 4.6. The curves are not drawn for the entire domain as the variable T_{thr} needed to be discretized due to the high non-linearity of the problem and the insurgence of some numerical instability around $v_\infty \to 0$.
From the bottom graph in fig. 4.6 the v_∞ appears to have a quasi-linear dependance from the time of thrust T_{thr}. A regression analysis is conducted to verify the accuracy with which the curves could be approximated by a straight line having the equation:

$$v_\infty = m * T_{thr} + q$$

The parameter R^2 in tables 4.2 and 4.3 is called coefficient of determination and represents the reliability with which the actual curve can be approximated by the regression line: the best result is obtained when $R^2 = 1$. Moreover, from the equation of the regression line, we can extrapolate the value of $T_{thr,max}$, which is the time of thrust that needs to be provided to, hypothetically, reach the best condition $v_\infty \approx 0$.

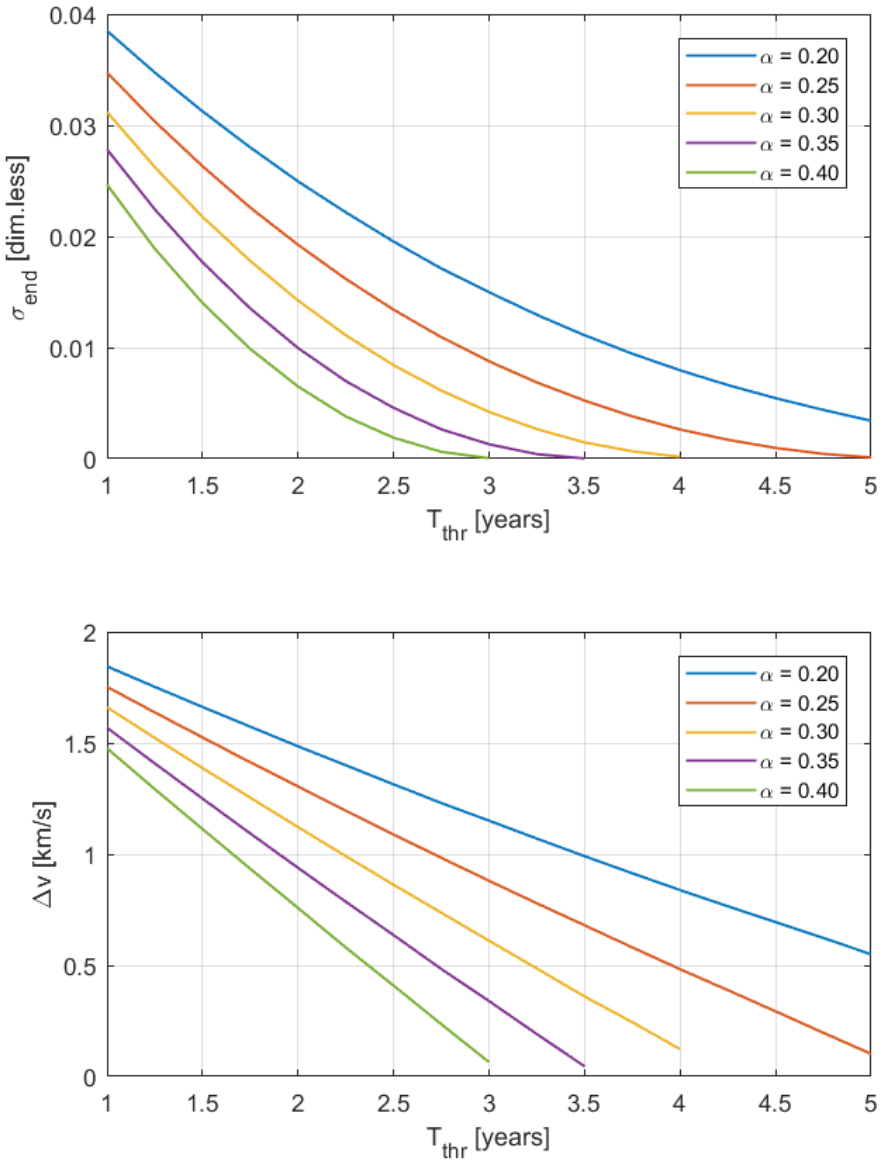

Figure 4.6: v_∞ as function of T_{thr} for different values of α

	m	q	R^2	$T_{thr,max}$ (ys)
$\alpha = 0.20$	-0.32317	2.13741	0.99834	6.614
$\alpha = 0.25$	-0.41143	2.13307	0.99903	5.185
$\alpha = 0.30$	-0.51230	2.15437	0.99957	4.205
$\alpha = 0.35$	-0.60861	2.16363	0.99975	3.555
$\alpha = 0.40$	-0.70551	2.17328	0.99989	3.080

Table 4.2: Regression line parameters calculated with all data points

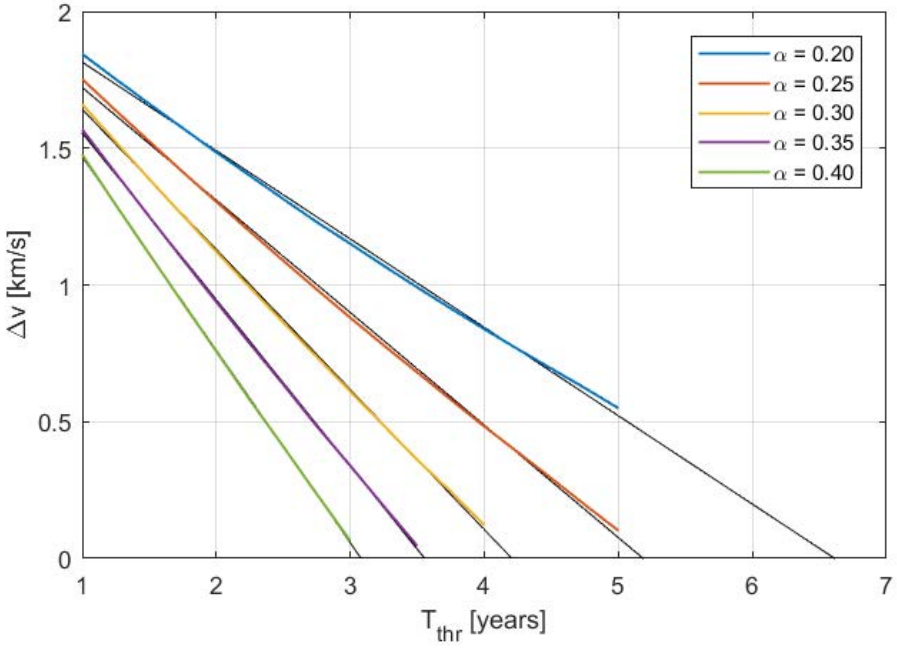

Figure 4.7: Regression line calculated with all data points

As can be visualized in fig. 4.7, there is a better concurrence between curve and regression line for higher values of α, but only because they were calculated for a smaller number of data points closer to the respective value of $T_{thr,max}$.

	m	q	R^2	$T_{thr,max}$ (ys)
$\alpha = 0.20$	-0.29024	2.00037	0.99991	6.892
$\alpha = 0.25$	-0.38258	2.01401	0.99998	5.264
$\alpha = 0.30$	-0.49077	2.08275	0.99980	4.244
$\alpha = 0.35$	-0.59212	2.11564	0.99993	3.573
$\alpha = 0.40$	-0.69587	2.14922	0.99995	3.089

Table 4.3: Regression line parameters calculated with last 5 data points

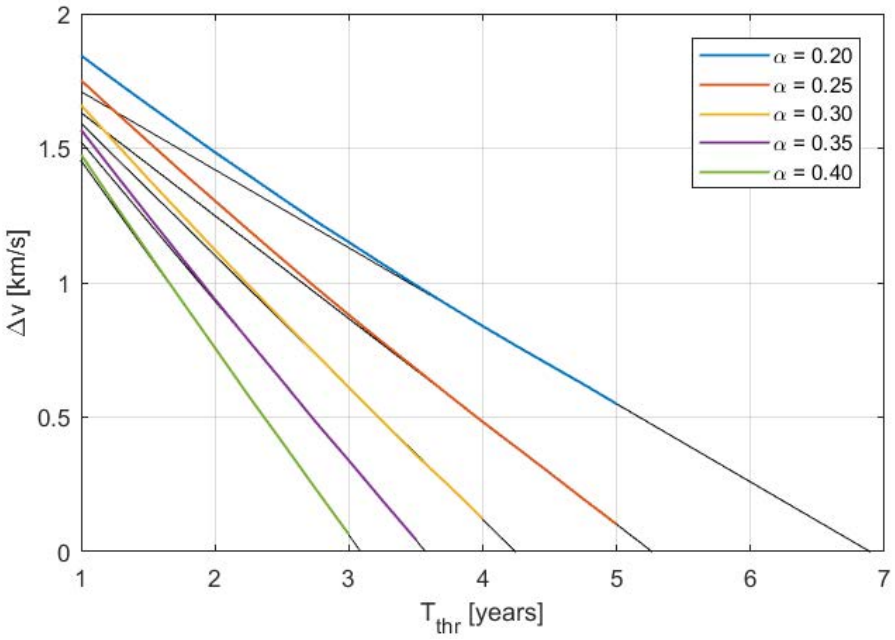

Figure 4.8: Regression line calculated with last 5 data points

A better estimate can be calculated utilizing, for each curve, only the last 5 data points, obtaining a regression line that approximates the slope of the curve at its final end (fig. 4.8). New simulations were run adopting, for each value of the acceleration, the $T_{thr,max}$ values extrapolated from table

4.3: the results are visualized in fig. 4.9, where the v_∞ is plotted versus the delay time δ. The best results, expressed in table 4.4, show that the v_∞ has been reduced by an additional order of magnitude, down to values of the order of 10 m/s. The results calculated from the extrapolated data for $T_{thr,max}$ do not produce $v_\infty = 0$ yet, meaning that there are errors that are implicit within the approximation, but with further iterations and more data points an exact final result could theoretically be calculated. Nevertheless, the results provided are already very good in the perspective of minimizing the relative velocity, and are only affected by the limitations given by the life expectancy of real electric thrusters.

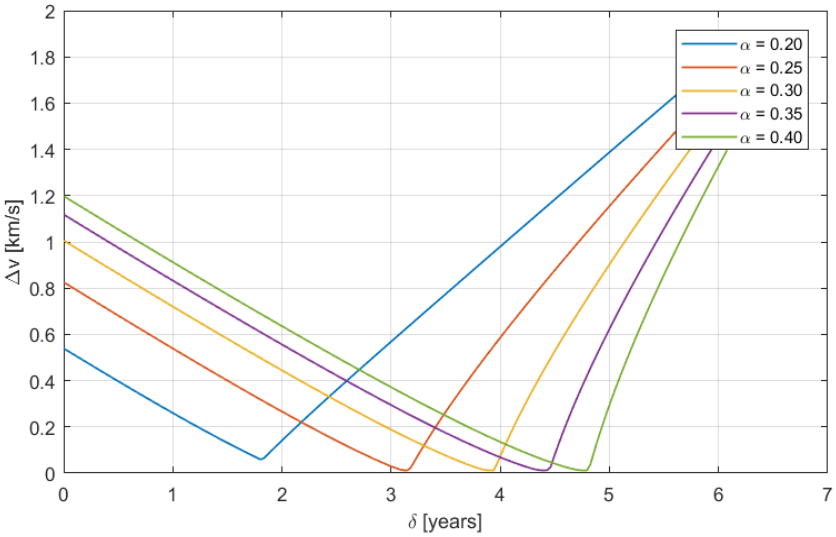

Figure 4.9: v_∞ versus δ with optimal value for T_{max}

	$\boldsymbol{T_{max}}$ (ys)	$\boldsymbol{v_{\infty,min}}$ (m/s)
$\alpha = 0.20$	6.892	59.50
$\alpha = 0.25$	5.264	11.83
$\alpha = 0.30$	4.244	11.72
$\alpha = 0.35$	3.573	11.68
$\alpha = 0.40$	3.089	11.67

Table 4.4: Near-zero v_∞ values for different accelerations

Chapter 5

Orbital Design of the Mission

In this section all the theory and the results developed so far will be applied to the real case of designing the mission to Saturn: the parameters of the design will not be speculative, but chosen from state-of-the-art pieces of technology to evaluate the feasibility of the mission and its cost/outcome ratio. The total mass of the spacecraft is assumed to be 1000 kg, while the initial orbital design is that presented in section 2.3 involving a pure flyby around Jupiter. The parameters of the transfer orbit are reported once again in table 5.1.

Transfer orbit 2			
e	0.455335	a	0.6873765
i	0.0	$\theta_{departure}$ (rad)	1.546061
ω (deg)	88.6728	$\theta_{arrival}$ (rad)	3.112125
Ω	/	ΔT	1.365526

Table 5.1: Dimensionless parameters of the Jupiter-to-Saturn transfer orbit

5.1 Choices for α and T_{thr}

A few words will be spent here on state-of-the-art technology concerning electric thrusters. Without getting into the details of the subject, which would be out of the purpose of this work, we want to outline some of the main features of electric thrusters to make a sensible choice about which one(s) would fit in with the current mission requirements. In electric propulsion, gas propellant is ionized and accelerated through electric and/or magnetic fields to produce a mass flow, which is the driving force of the thrust. The ionized particles are ejected very fast compared to the speeds that can be reached with chemical propulsion, resulting in a much higher *Specific Impulse* $I_{sp} = v_{out}/g$; on the other hand, the mass of the ionized gas is considerably smaller compared to that of solid or liquid propellants in chemical motors, making the net thrust several orders of magnitude lower. The main advantage of electric propulsion is that the gas propellant is much lighter and easier to deal with in space, resulting in lower launch costs and avoiding attitude-related problems such as the sloshing of liquid fuel inside tanks. The main drawback of electric propulsion is, though, the necessity of having a strong and stable source of power that sustains the electro-magnetic field. This can be easily done in Earth orbits, as the proximity of the Sun makes the problem readily solved with solar arrays: the solar constant $J = 1350$ W/m^2 provides a power output higher than 1 kW with only one m^2 of solar arrays. With the intensity of the solar radiation decreasing proportionally to the distance R^{-2}, it goes from approximately $J = 50$ W/m^2 at Jupiter's orbit to $J = 13.5$ W/m^2 at Saturn's orbit, making it quite difficult to generate power from sunlight with solar arrays without having a huge impact on the mass budget. The best way to provide for the thruster's and the satellite's power needs throughout the mission is given by *Radioisotope Thermoelectric Generators (RTG's)*: these consist of a certain number of devices called *General Purpose Heating Source (GPHS)*, which exploit the natural decay of

Plutonium 238 to produce thermal power. Each module of GPHS contains four pellets of Pu-238 which produce 62.5 W_t each, for a total nominal output of 250 W_t per module and a weight of approximately 1.43 kg [22].

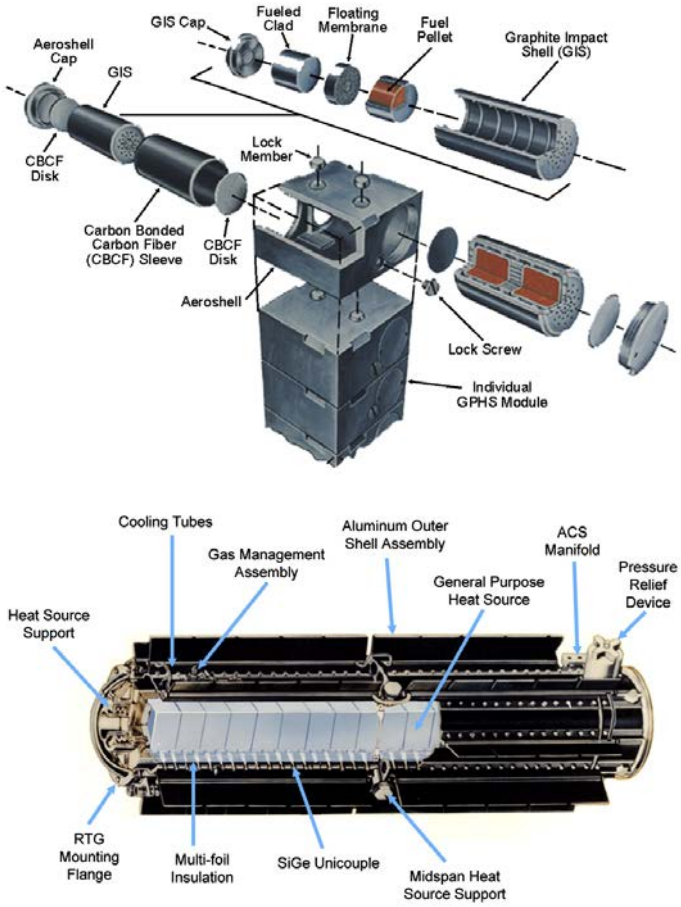

Figure 5.1: GPHS unit (above) and RTG assemble (below) [22]

Thermal power can be converted into electric power through the Seebeck effect, according to which when heat is transferred to the electric junction of two different conductive materials it generates a voltage difference, which results in electric current when connected to a load. State of the art GPHS-

RTG's contain a stack of 18 modules that can produce an electric power output of 285 W_e at launch and weigh 55.9 kg [22]. These models of RTG's were utilized in both the Galileo and Cassini missions: the first one visited Jupiter and was equipped with 2 RTG's, the second visited Saturn and was equipped with 3 RTG's [23]. In both cases, the generators worked continuously until the end of both missions, which lasted almost 14 years and 20 years respectively. Losses of power of around 7 W per year are to be expected, because of the progressive decay of Plutonium and the degradation of Si-Ge thermocouples [23]. The appropriate thruster is therefore to be selected according to its total power consumption, which needs to match the capabilities of the RTG's: assuming to install two RTGs to supply for the thruster and the satellite's other needs, a good choice would imply a power requirement of 300-400 W maximum; within this upper bound, any thruster that can provide the maximum thrust is eligible for the choice, as a higher thrust allows to reach a lower v_∞. Good choices might be the BHT-200 by Busek, the HiVHAc developed by NASA, and the SPT-50 by OKB Fakel [19]. Another interesting and newer model is the PPS®X00 currently being developed at Safran: this Hall thruster is being designed to work within the power range of [200,1000] W to meet a variety of performance requirements; the optimal design point is at 650 W, providing 40 mN of thrust with an efficiency equal to that of the best state-of-the-art models available [24]. The PPS®X00 is expected to become available on the market by 2020 [24]; looking at the operating envelope in fig. 5.2 we can get an estimate of the thrust available with our problem constraints: assuming to use this thruster for the mission, with a power input of 300 W we read a thrust output of 19 mN and a specific impulse of 1150 s, since we are interested in maximizing the thrust. This leads to the definition of the acceleration $\alpha = 0.3228$, which falls in the range of parameters previously investigated. As for the choice of T_{thr} we plan on using only one thruster, and for lack of a better estimate we assume a total functioning time of 2.5 years [20, 21].

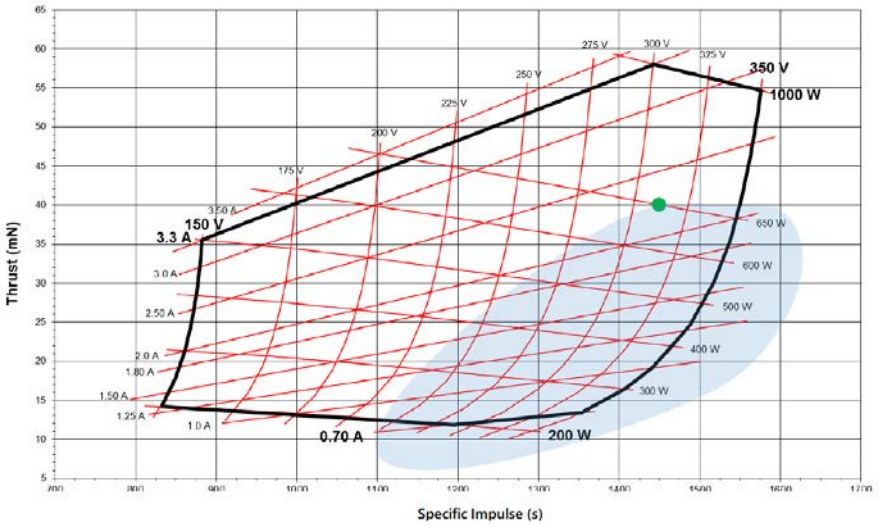

Figure 5.2: Operating envelope of the PPS®X00. Blue area: stare-of-the-art thrusters currently available [24]

5.2 Launch windows

The problem is implemented and integrated with the choice of variables described in the previous sections; the value for δ is that of best choice and results in $\delta^* = 0.967336 = 4.89789$ years. The orbital design is visualized in fig. 5.3, from which it can be noted that another problem arises: Saturn's altitude is reached and the tangency condition is satisfied, but the thrust arc produced a delay in the total time of flight and in the longitude l of the spacecraft at the end of the integration. The spacecraft reaches the desired altitude in a total time of $T_{tot} = 7.397$ years and spanning an angle of $\Delta\theta = 1.6749$ rad. The next step will be finding the optimal instant in which the flyby around Jupiter is to be performed, in order to reach the exact same position as Saturn in the desired time: in other words, finding the optimal launch window for the transfer orbit. This will require to reiterate the problem and the time windows previously calculated.

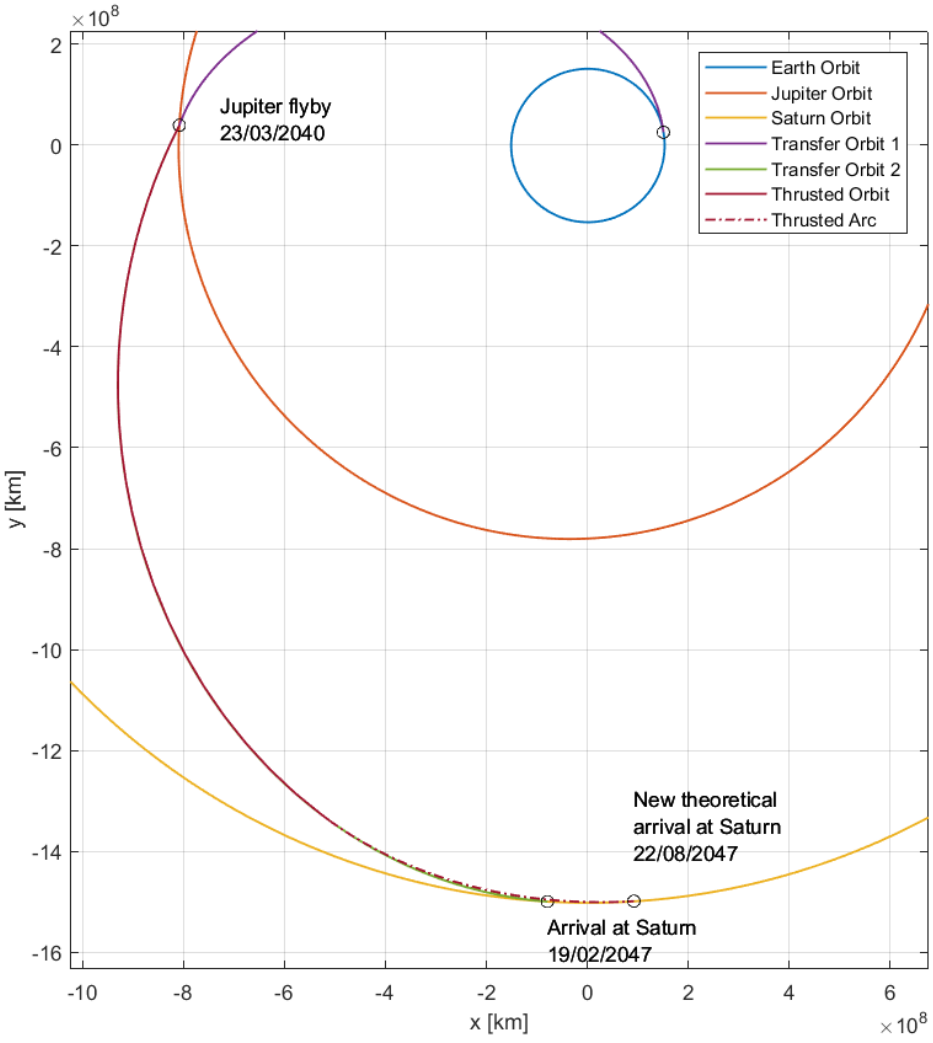

Figure 5.3: Non-thrust and thrust transfer orbits

5.2.1 Circular orbits approximation

When assuming that planetary orbits are circular, the longitude of the orbiting body is given by a linear relation:

$$l(t) = l_0 + \omega t$$

where l_0 is the initial position and ω the mean motion. In our case, on 23/03/2040:

$$\begin{aligned} l_{0J} &= 3.0937 & \omega_J &= 1.69 \cdot 10^{-8} \text{ rad/s} \\ l_{0S} &= 3.2807 & \omega_S &= 6.77 \cdot 10^{-9} \text{ rad/s} \end{aligned}$$

and the requirements are: $\Delta l_{JS} = 1.6749$ rad and $T_{tot} = 7.397$ years. The following relation needs to be satisfied:

$$\Delta l_{JS} + 2k\pi = l_S(t + \Delta T_{tot}) - l_J(t) = \Delta l_0 + \omega_S \Delta T_{tot} + (\omega_S - \omega_J)t$$

$$\begin{cases} t = \dfrac{\Delta l_{JS} - \Delta l_0 - \omega_S \Delta T_{tot}}{\omega_S - \omega_J} + kT_{JS} \\ T_{JS} = \dfrac{2\pi}{\omega_J - \omega_S} = 6.2037 \cdot 10^8 \text{ s} \end{cases}$$

meaning that the desired condition repeats every $T_{JS} = 19.672$ years.

5.2.2 Elliptic orbits

When handling elliptic orbits, the method presented above only provides an estimate of the good launch window, but cannot calculate it with precision as the mean motions of the planets vary with their positions along the trajectory. To obtain a more precise solution it is possible to use the Differential Evolution algorithm with a few modifications:

- $T_2 = T_{JS}$: the third element of the decision vector $\boldsymbol{X}$ is imposed to be equal to the total desired time of flight for each member of the initial

population. This way, newer individuals will evolve adapting the first two components, while the third one will remain fixed at the desired value.

- $C = |\Delta\theta - \Delta l_{JS}|$: the cost function is calculated as the difference between the desired Δl_{JS} and the angle $\Delta\theta$ spanned by a hypothetical transfer orbit that links Jupiter and Saturn without a thrust arc.

The solution can be calculated with an absolute error that is lower than $\epsilon_l = 10^{-15}$, while the T_{JS} remains unaltered.

5.2.3 Comments

Changing the time variables of the problem is necessary to physically encounter the target planet. The main problem is that this method does not produce optimal conditions for the flyby: finding the best launch window to optimize the thrust trajectory makes it impossible to launch the spacecraft from the Earth and realize a free flyby around Jupiter without implementing trajectory corrections along the way. This problem will be discussed further in this chapter, for now it will suffice to keep it in mind. One additional issue is that, in order to meet the target planet with the procedure outlined so far, the keplerian parameters of the spacecraft at its departure from Jupiter in the newly calculated launch window need to be the same as in the case expressed by table 5.1 and fig. 5.3. This is virtually impossible, as the newly calculated radius of the spacecraft, coinciding with Jupiter's position vector, will be slightly different from before, due to the ellipticity of Jupiter's orbit. The outgoing transfer orbit is computed as follows:

- e and a: remain unchanged;
- θ: it is calculated from the parameters e and a and the current radius of Jupiter r_J;

- $\omega = l_J - \theta$

This technique still produces slight errors in the total flight time T_{JS}, as the true anomaly of the departing S/C, calculated from Jupiter's real radius, is slightly different from that in table 5.1. This problem is solved iteratively: for each iteration new values of T_{JS} and Δl_{JS} are calculated, from which the corresponding launch window can be found through the DE algorithm. At each iteration, the errors in the two parameters decrease as the optimal solution is approached.

5.3 Results

Transfer orbit 2			
Jupiter Flyby	08/03/2040	Arrival at Saturn	26/08/2047
e	0.455335	a (km)	$1.03195 \cdot 10^9$
i	0.0	$\theta_{departure}$ (rad)	1.545474
ω (deg)	87.4732	ΔT (ys)	7.47279

Table 5.2: Parameters of the final Jupiter-to-Saturn transfer orbit

After a few iterations, the problem converges. The parameters of the transfer orbit from Jupiter to Saturn are reported in table 5.2. The thruster is turned on after $\delta^* = 0.98139 = 4.97065$ years; with the engine working continuously for 2.5 years, there appears to be a small mismatch with the total flight time, probably due to numerical imprecisions. This results in almost 19 extra hours of unpowered flight before actually reaching Saturn: the error is acceptable for now, compared with the time scales involved, and can be optimized with more powerful calculators. The final trajectory can be visualized in fig. 5.4, where the green transfer trajectory is the hypothetical solution to Lambert's problem than connects Jupiter and Saturn in the same time, but without the thrust arc.

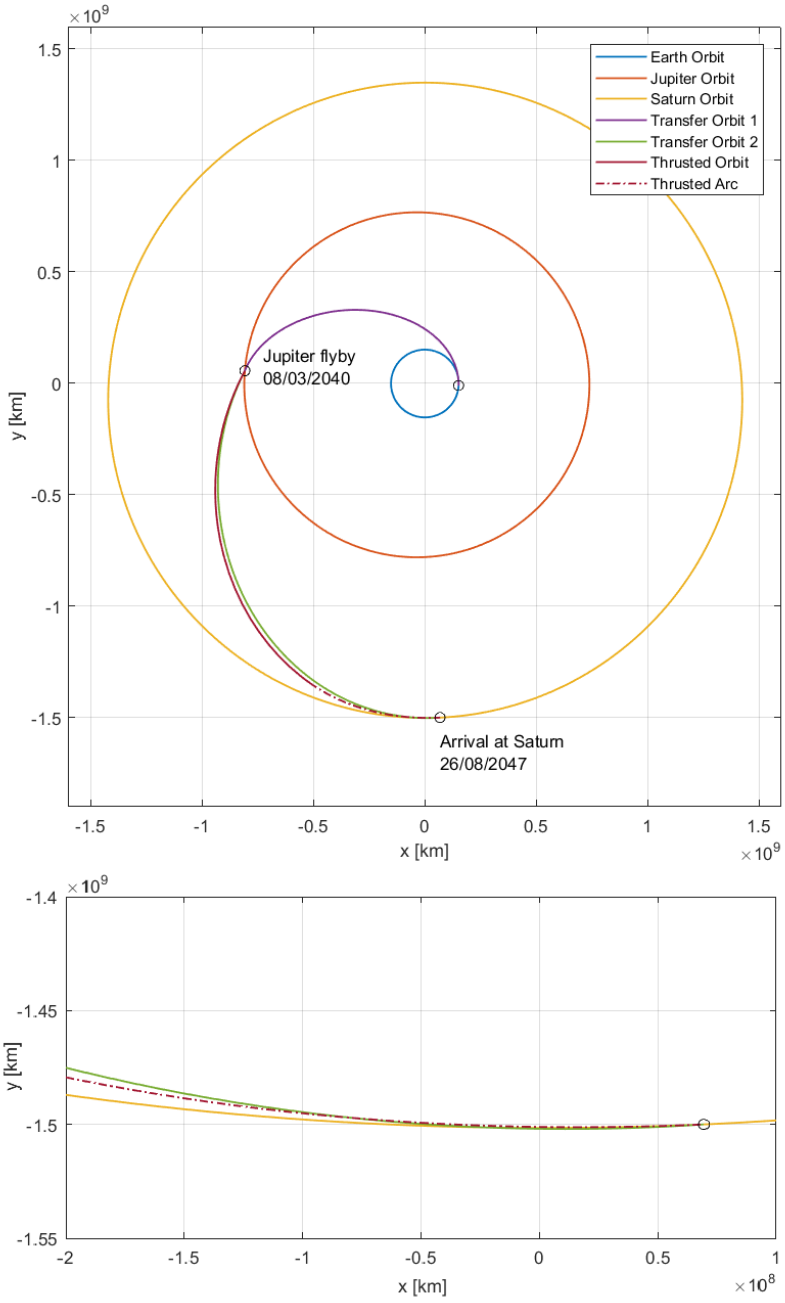

Figure 5.4: Final transfer orbit with thrust arc

The orbit with the thrust arc offers a better solution to the problem of approaching Saturn, as it can be seen from the figure, because it is tangent to Saturn's orbit at the intersection point, while the normal transfer orbit is not. The green trajectory reaches Saturn with $v_\infty = 2.12135$ km/s, while with the final design for the thrust orbit the hyperbolic excess speed is reduced to:

$$v_\infty = 0.75696126 \text{ km/s}$$

The final solution is affected by some numerical imperfections, which can ideally be reduced to near-zero values with better numerical precision and more iterations. The absolute errors on the ΔT_{JS} and the Δl_{JS}, which are the subjects of the iterations, are the following:

- $\epsilon_{\Delta T} = -416.97$ s: the S/C reaches the desired altitude 7 minutes before the expected time;
- $\epsilon_{\Delta l} = 4.099 \cdot 10^{-08}$: there is an difference of about 66.55 km along the perpendicular direction between the final position of the S/C and the position occupied by Saturn (the equatorial radius of Saturn is $R_S = 58232$ km).

The keplerian osculating parameters, the angle of thrust β and the parameter σ are represented in 5.5. Both a and p increase over time, while e decreases because the orbit is being circularized. The angle β is defined only in the thrust segment and equal to zero otherwise; at the end of the thrust leg the optimal thrust angle is $\beta = 0$, meaning that to further reduce the relative speed, an impulse should be given along the tangential direction, as the S/C and Saturn are in the same position. The parameter σ, as representative of the relative velocity, diminishes as it is expected to.

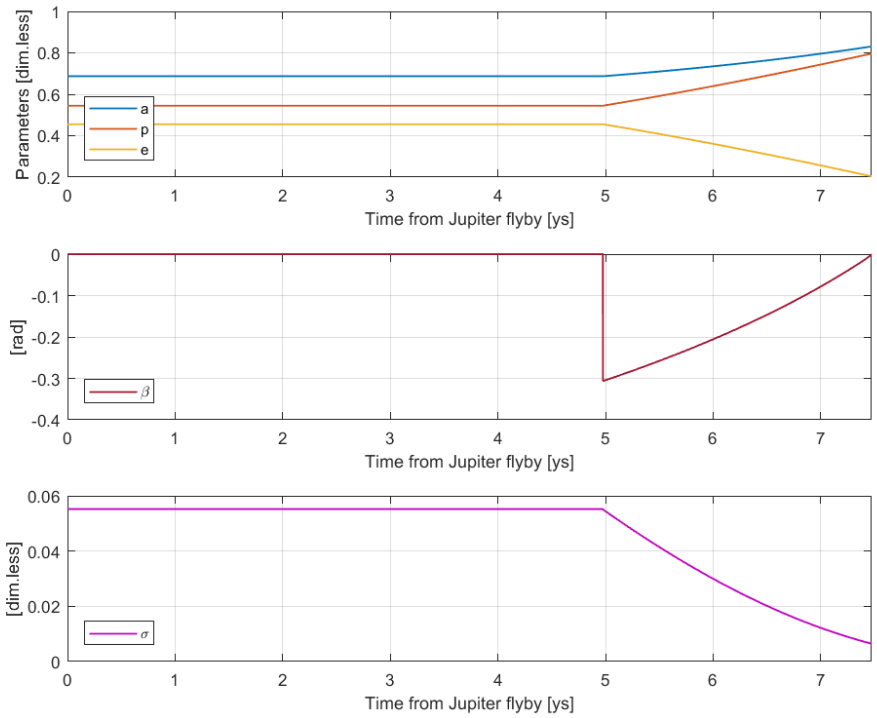

Figure 5.5: Final transfer orbit with thrust arc

5.4 Redefinition of Transfer Orbit 1

As mentioned previously, recalculating the optimal time and position for the flyby in Jupiter requires modifications to the Transfer Orbit from the Earth, as the orbit calculated in previous sections does not match the new requirements. Two options are explored to solve the problem: the first one involves a powered flyby around Jupiter to meet the v_∞ requirement at the exit of the sphere of influence, the second one consists in a free flyby around Jupiter, but requires a D.S.M. to inject the S/C into the appropriate transfer

orbit that leads to said free flyby. In none of the cases will it be possible to perform the entire mission without Δv adjustments.

Powered Flyby

The solution with a powered flyby is obtained pruning the domain looking for the solution that would grant both the minimum difference between the v_∞ at arrival and departure from Jupiter, and the minimum Δv to be provided by the launcher when departing from the Earth. The parameters of the best solution found are summarized in table 5.3:

Transfer orbit 1			
Earth Departure	30/09/2037	Jupiter Flyby	08/03/2040
Δv_{BO} (km/s)	6.4972	$v_{\infty,J}^{in}$ (km/s)	5.7309
e	0.68939	a (km)	$4.9075 \cdot 10^8$
ω (deg)	4.6672	$\theta_{departure}$ (rad)	-0.14972
ΔT (ys)	2.4385	$\theta_{arrival}$ (rad)	2.9907

Table 5.3: Parameters of the Earth-to-Jupiter transfer orbit

The solution calculated in the previous section 5.3 consisted in a $v_{\infty,J}^{out} = 5.3917$ km/s, which should be equal to the $v_{\infty,J}^{in}$ to allow for an unpowered flyby: hence the necessity of a corrective maneuver. The corrective impulse of $\Delta v = -0.170$ km/s is applied at the perijove at a radius of $r_P = 2.7823 \cdot 10^6$ km. This maneuver, assuming a post-burn mass of $m_{S/C} = 1000$ kg, would burn approximately 60 kg of fuel mass, if realized by a liquid-propellant thruster of $I_{sp} \approx 300s$. The amount of fuel required is acceptable, but cannot overcome the necessity of carrying a liquid engine and its own inert mass all the way to Jupiter.

D.S.M. and pure Flyby

To have an unpowered flyby around Jupiter, the S/C needs to reach the planet with a hyperbolic excess speed of exactly $v_\infty = 5.3917$ km/s. For this purpose, the theory outlined in section 3.2 can be applied: using Jupiter's radius as scale length a_0, we draw a curve $\Gamma^J_{\phi,\psi}$ referred to Jupiter following the formulation in section 3.2.2, and a curve Γ^E referred to the Earth, according to the formulation in section 3.2.1 and assuming a circular orbit for the Earth in first approximation. A third curve, in green in fig. 5.6, describes the locus of points that represent orbits that intersect Jupiter with the desired v_∞, meaning $\sigma = 0.1771$. The intersection between the green

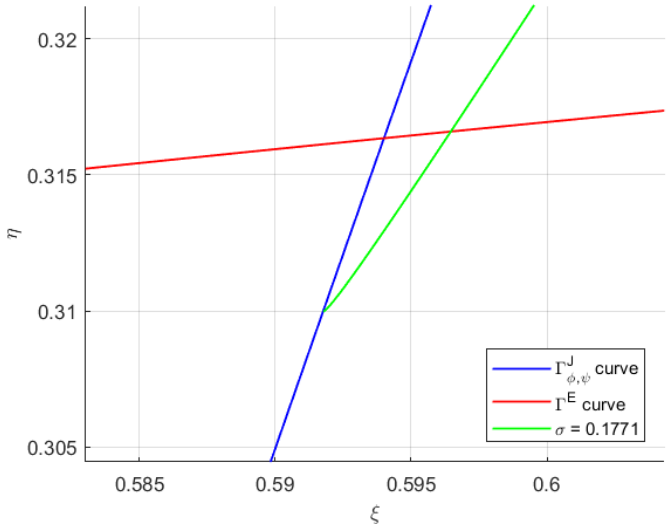

Figure 5.6: ξ and η parameters of the Earth-to-Jupiter transfer orbit

and red curves corresponds to the orbit that reaches Jupiter with the desired relative velocity and is quasi-tangent to the Earth's orbit. Its parameters are reported in table 5.4. The problem with this second option is that it is not possible to launch the S/C directly into this orbit, because the flight time between the launch from the Earth and the arrival at Jupiter might,

Transfer orbit 1			
Earth Departure	TBD	Jupiter Flyby	08/03/2040
e	0.68499	a (km)	$4.8234 \cdot 10^8$
ω (deg)	-0.08	$\theta_{arrival}$ (rad)	3.07355

Table 5.4: Parameters of the Earth-to-Jupiter transfer orbit

in general, not be equal to the flight time required to reach Jupiter on the 08/03/2040. For this reason, it might be necessary to put the S/C into a parking orbit around the Sun, with an optimal phase angle with respect to the Earth, or launch the S/C into an orbit that intersects the target orbit in table 5.4, provide a Δv to acquire it. In any case, the best solution needs to get the spacecraft to Jupiter in the desired time, and minimize the sum of Δv's of launch and D.S.M. The solution will not be presented here. The two solutions (from table 5.3 and 5.4 can be visualized in fig. 5.7.

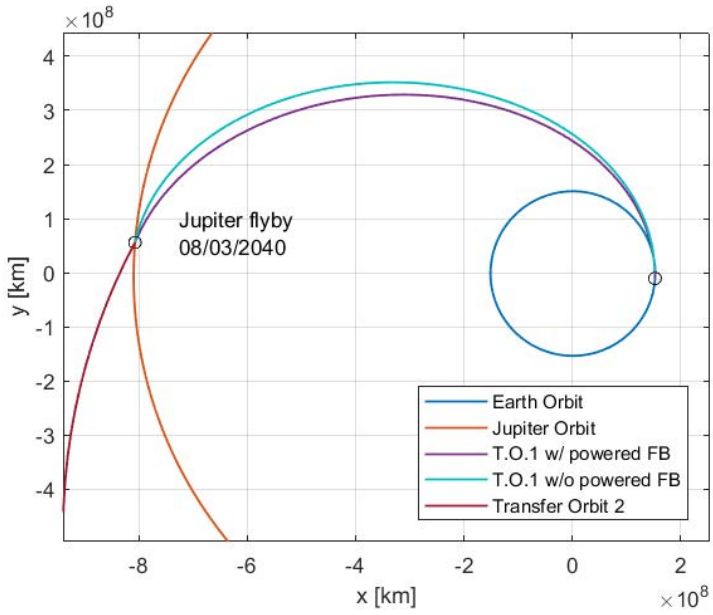

Figure 5.7: Comparison between the two solutions for the T.O.1

Chapter 6

Capture

In the previous chapters, the aim was to reduce the relative speed between the spacecraft and Saturn at the encounter. In this sections we want to describe the real benefits of this choice, which consist in easing the capture procedure of the spacecraft into Saturn's gravity field. To avoid further propellant consumption the capture will be performed by an Electrodynamic Tether (EDT); the study of feasibility carried out in the following pages will not be strictly rigorous, and will follow the procedures outlined by E. C. Lorenzini and J. R. Sanmartín, the main experts and leading researchers in the field of EDT's for space applications. The first Tethered Satellite System was proposed to NASA and the Italian Space Agency in the 1970's by Mario Grossi, from the Smithsonian Astrophysical Observatory, and Giuseppe Colombo, from University of Padua (Italy) [25]. A Tethered Satellite System consists of a satellite with a metallic cable incorporated and coiled during launch, which needs to be deployed to perform the designated operations. The tether can extend up to several dozens of kilometers (up to 300 km), depending on the application [25]; tethers can be used to provide attitude stabilization and control, perform orbital maneuvers and generate power through interactions with space environmental plasma.

6.1 Stability of Inert Tethers

We analyze briefly the dynamics of an *Inert Tether*, which is a tether that does not interact electrically with the surrounding space environment and is only subjected to the main gravity field. Once the satellite is positioned into orbit and the tether is deployed, the orbital motion is described by the system's gravity center. Since gravity does not vary linearly with altitude, the center of gravity does not generally coincide with the center of mass, and said displacement becomes more evident the longer the tether is; for a satellite consisting in two equal masses $m_1 = m_2 = m$ and a tether length that is relatively small compared to the orbital radius, center of mass and center of gravity can be assumed to coincide [25]. The situation depicted in figure 6.1

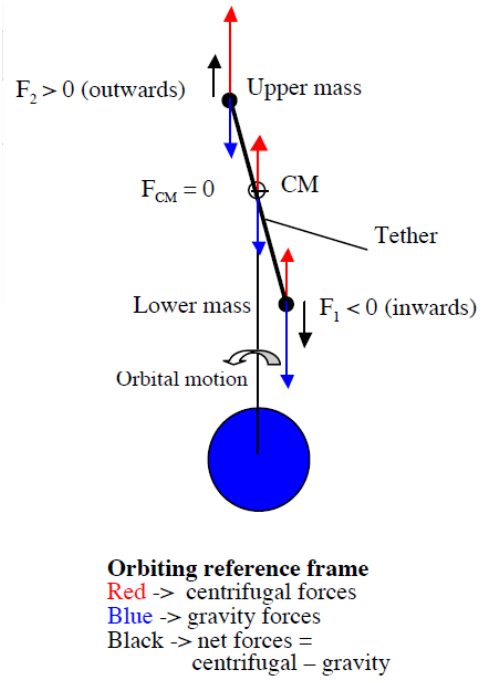

Figure 6.1: Inert Tether in orbit [26]

explains the net forces acting on the system: the lower mass m_1 experiences a stronger gravity force because it is closer to the main gravity field, but on the other hand, being forced to rotate at the center's orbital velocity ω_0 at a lower altitude, it experiences a lower centrifugal force. The opposite situation happens to the higher mass m_2. The net forces are counterbalanced by the tension T on the tether, and the oscillations of the system due to the gravity gradient are called *librations*. The motion of the single mass m around the center of mass can be studied through the equations of proximity of Clohessy-Wiltshire, where the mass is deployed in the orbital plane and the only external force acting on it is the tension along the tether [26]:

$$\begin{cases} \delta\ddot{x} - 3n^2\delta x - 2n\delta\dot{y} = f_x \\ \delta\ddot{y} + 2n\delta\dot{x} = f_y \end{cases}$$

where δx and δy are the coordinates of the mass with respect to the CM in the orbital frame and f_i the components of the tension per unit mass:

$$\begin{cases} f_x = -\dfrac{T\cos\theta}{m} \\ f_y = -\dfrac{T\sin\theta}{m} \end{cases}$$

Adopting polar coordinates $\delta x = l\cos\theta$ and $\delta y = l\sin\theta$ and assuming the tether to be fully deployed ($\dot{l} = 0$) leads to the following equation for the libration angle θ around the local vertical [26]:

$$\ddot{\theta} + 3n^2\sin\theta\cos\theta = 0$$

from which we compute the pulsation of the oscillation $\omega_0 = \sqrt{3}n$. Imposing the condition $\ddot{\theta} = 0$ leads to the positions of equilibrium $\theta = k\frac{\pi}{2}$ with $k = 0, ..., 3$; assuming that the system is librating around one of the positions of equilibrium θ_0 we obtain:

$$\ddot{\theta} + 3n^2\sin(\theta_0 + \theta)\cos(\theta_0 + \theta) = 0$$

from which it can be demonstrated that the only stable positions of equilibrium are for $\theta_0 = 0$ and $\theta_0 = \pi$, because they produce a positive sign for the damping term [26], otherwise the libration is amplified. The system is therefore stable only when aligned with the local vertical.

6.2 Electrodynamic Tethers

6.2.1 Generalities

An Electrodynamic Tether (EDT) consists of a tether made of conductive material which can interact with the planet's electromagnetic field through the insurgence of an electric field $\vec{\boldsymbol{E}}_m$ in the orbital frame, which is due to the relative motion of the spacecraft and the planetary magnetic field $\vec{\boldsymbol{B}}$. The electric field can be calculated as [27, 28]:

$$\vec{\boldsymbol{E}}_m = (\vec{\boldsymbol{v}}_{s/c} - \vec{\boldsymbol{v}}_{pl}) \times \vec{\boldsymbol{B}}$$

where $\vec{\boldsymbol{v}}_{pl}$ is the velocity of the plasma, which corotates around the planet with the planet itself [28]. Therefore, considering a satellite into a circular equatorial orbit, it is possible to define an orbital radius at which the electric field changes direction: this corresponds to the stationary radius [28]:

$$a_s = \sqrt[3]{\frac{\mu_S}{\Omega_S^2}}$$

with μ_S and Ω_S being the planet's gravity constant and rotational angular velocity respectively. At $r = a_s$ the relative velocity is zero and there is no induced electric field; in all other cases, the electric field produces a current I on the conductive tether: the current interacts with the magnetic field giving rise to a Lorentz drag force with the expression [27] [28]:

$$\vec{\boldsymbol{F}} = I\vec{\boldsymbol{l}} \times \vec{\boldsymbol{B}}$$

where $\vec{\boldsymbol{l}}$ is directed along the tether length and oriented according to $\vec{\boldsymbol{E}}_m$. It can be easily shown that for an equatorial circular orbit having $r < a_s$

the Lorentz force acts in the opposite direction to that of the spacecraft's velocity, resulting in a sort of a viscous drag, while for $r > a_s$ the force acts in the same direction as that of the spacecraft's velocity. Obviously with the aim of having the S/C captured by the planet, we want it to pass as close as possible to the planet to have the Lorentz force acting as a drag and reducing the orbit's eccentricity to a value lower than 1. In the case of this study, the S/C will enter the planet's sphere of influence into an orbit that will be barely hyperbolic [28], thus the $\vec{\boldsymbol{v}}_{s/c}$ vector will have a radial component and the discriminating radius a_s will not correspond to the stationary radius; assuming the injection orbit to be parabolic, the new discriminating radius can be calculated as [28, 29]:

$$r_M = a_s \sqrt{\frac{2a_s}{r_P}}$$

with r_P being the periapse radius. r_M is the radius below which the Lorentz force acts as a drag.

6.2.2 The bare tether

We have so far explained the insurgence of an electric field $\vec{\boldsymbol{E}}_m$ when the TSS moves relatively to the ambient plasma. To allow a current I to flow along the tether, the circuit needs to be closed, and the way to do so is through the ambient plasma itself [25]. Early EDT designs involved a big conductive sphere at one end of the tether to work as the anode and collect electrons from the plasma, while on the other side an electron gun would eject those electrons back into the environment [30]: in this design, the tether acts as an impedance between the two ends, but stays insulated from the environment. The bare tether concept was suggested later in the 1990's to allow a larger electron collection: the tether would be left bare (free of insulation) and free to interact with the ambient plasma, therefore acting like a gigantic and efficient Langmuir probe with a small cross section compared to the length,

that can extend up to tenths of kilometers [30]. The current induced on the tether is the so called orbital-motion-limited current I_{OML}. This current is limited by the tether's short circuit value $\sigma_c E_m A$ and is a function of a characteristic length L_{ch}, which gauges ohmic effects on the bare tether [30]. The expression for L_{ch} is [30]:

$$\frac{4}{3} e N_e \frac{p L_{ch}}{\pi} \sqrt{\frac{2 e E_m L_{ch}}{m_e}} = \sigma_c E_m A$$

where the following terms are involved:

- e, m_e, N_e: electron charge, mass and density in the plasma environment respectively;
- p: perimeter of the tether;
- A: cross section of the tether;
- σ_c: electric conductivity of the tether.

Since it is more convenient to obtain lower values for L_{ch} (as will be shown later on), the preferable shape of the tether is that of a tape of width w and thickness h, to reduce the A/p ratio. For a thickness h that's negligible compared to the width, the expression above reduces to [29]:

$$\frac{4}{3} e N_e \frac{2 w L_{ch}}{\pi} \sqrt{\frac{2 e E_m L_{ch}}{m_e}} = \sigma_c E_m w h \Longrightarrow L_{ch} \propto \frac{h^{2/3} E_m^{1/3}}{N_e^{2/3}}$$

The I_{OML} current can be calculated through a length-averaged current value i_{av} [29]:

$$\frac{I_{OML}}{\sigma_c E_m w h} = i_{av} \left(\frac{L}{L_{ch}} \right)$$

where a small i_{av} corresponds to negligible ohmic effects and $i_{av} \approx 1$ to dominant ohmic effects. The value of i_{av} as function of L/L_{ch} (with L being

the actual tether length) can be approximated by the following expressions [29], while the exact function is visualized in fig. 6.2:

$$i_{av} = \begin{cases} 0.3(L/L_{ch})^{3/2} & \text{for } L/L_{ch} \ll 1 \\ L/4L_{ch} & \text{for } L/L_{ch} \leq 2 \\ 1 - L_{ch}/L & \text{for } L/L_{ch} > 2 \end{cases}$$

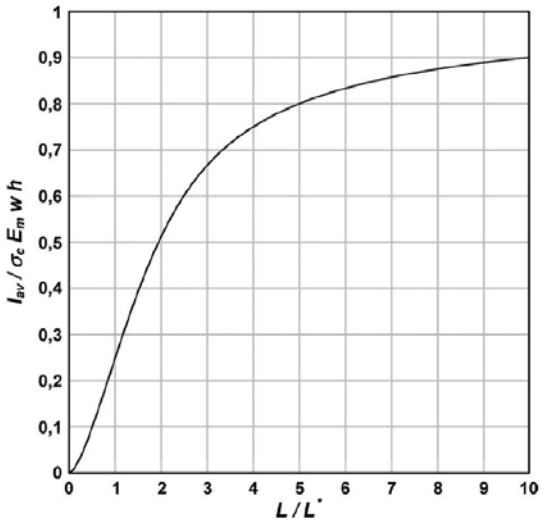

Figure 6.2: Normalized current i_{av} versus normalized tether length L/L_{ch} [28]

6.2.3 Saturnian Space Environment

As it has been highlighted in the previous chapters, the capture operation performed by an Electrodynamic Tether strongly depends on the planetary space environment, namely on the magnetic field $\vec{\boldsymbol{B}}$ and the electron density of the ambient plasma N_e. These factors are not yet very well known; here we will provide some information over the most up-to-date data, collected

during the Cassini mission and recently elaborated. Very simple models for the two quantities will be proposed.

Magnetic Field $\vec{B}$

Saturn's magnetic field is significantly weaker than Jupiter's: most studies involving EDT planetary captures found in literature are performed around Jupiter, and this poses the first challenge to the performance of the system around Saturn. The magnetic field $\vec{\boldsymbol{B}}$ is involved twice in the computation of the drag force which, in first approximation, leads to a squared-proportionality law between F and B. The magnetic field measured on Saturn's surface is $B_0 = 21160$ nT [31]; considering Saturn's equatorial radius $R_S = 60268$ km leads to a magnetic dipole moment of:

$$|\vec{\boldsymbol{m}}| = 4.632 \cdot 10^9 \text{ T} \cdot \text{km}^3$$

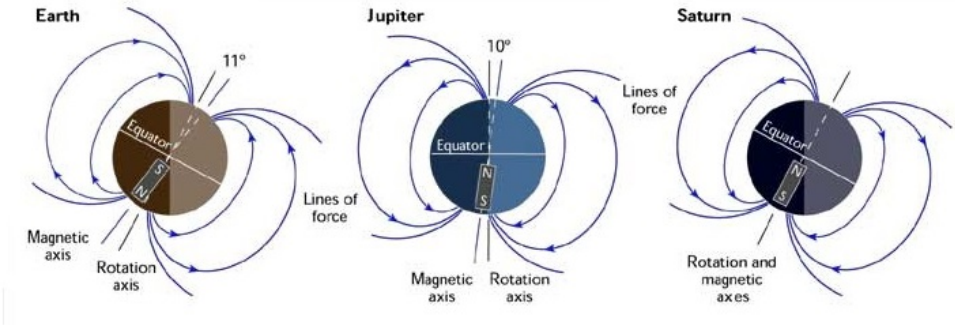

Figure 6.3: Sketches of the Earth's, Jupiter's and Saturn's magnetic field lines

The magnetic dipole moment vector $\vec{\boldsymbol{m}}$ has a tilt of less than 1° from Saturn's spin axis, and has an offset of 0.04 ± 0.02 R_S along the same axis [31]; for the purpose of this study the vector will be assumed to lie on the spin axis,

along the positive z-axis of a Saturn-centric equatorial frame. Contrarily to what happens on the Earth, the field lines of Saturn's magnetic field point downwards. With $\vec{\boldsymbol{r}}$ being the orbital radius expressed in equatorial coordinates, the vector $\vec{\boldsymbol{B}}$ follows from the 3D dipole law:

$$\vec{\boldsymbol{B}} = 3\frac{(\vec{\boldsymbol{m}} \cdot \vec{\boldsymbol{r}})}{r^5}\vec{\boldsymbol{r}} - \frac{\vec{\boldsymbol{m}}}{r^3}$$

Electron Density N_e

The plasma environment around Saturn in extremely diverse and articulated: it is complicated to provide a model that describes N_e with precision without neglecting some aspects that concur to the complexity of the phenomenon. The most detailed and up-to-date information about Saturn's plasma ambient come from the observations of the spacecraft Cassini; we will provide a brief description of Saturn's outer magnetosphere and plasmasphere, and secondly of its inner plasmasphere. Cassini was put onto Saturnian orbit in July 2004, and the high ellipticity of the orbit allowed repeated studies of the plasma populations in a broad range of radii from the planet's center of mass. Subsequent orbits were analyzed from December 2004 to March 2005, over which the spacecraft maintained an out-of-plane displacement from the planet's equatorial plane within $\pm 0.4 R_S$ [32]. The data from five different orbits show a radial dependance in the electron density, with a maximum around $5R_S$ and good repeatability and small scatter farther beyond [32]. The density profiles inside the $5R_S$ boundary are highly scattered (fig. 6.4). This phenomenon suggests a plasma source injection into the planet's environment, which reaches steady-state around $5R_S$ and distributes outwards uniformly [32]; one unconfirmed possibility is that the moon Enceladus might be itself the responsible for the plasma injection [32]. A simple power law can be used to approximate the regular behavior of plasma density N_e versus

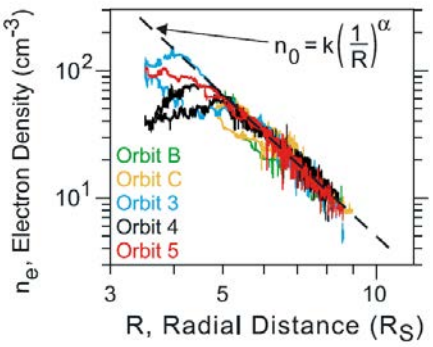

Figure 6.4: Electron density profiles per each orbit [32]

the radial distance, expressed in Saturn radii [32]:

$$N_e = k\left(\frac{1}{R}\right)^{\alpha} \text{ with } \begin{cases} k = 2.2 \cdot 10^4 \text{ cm}^{-3} \\ \alpha = 3.63 \pm 0.05 \end{cases}$$

This simple model also finds validation in the elaboration of Schippers [33], within the so called "Region 1" of the outer magnetosphere (fig. 6.5), where data from several orbits were merged together into one curve that expresses the radial dependance.

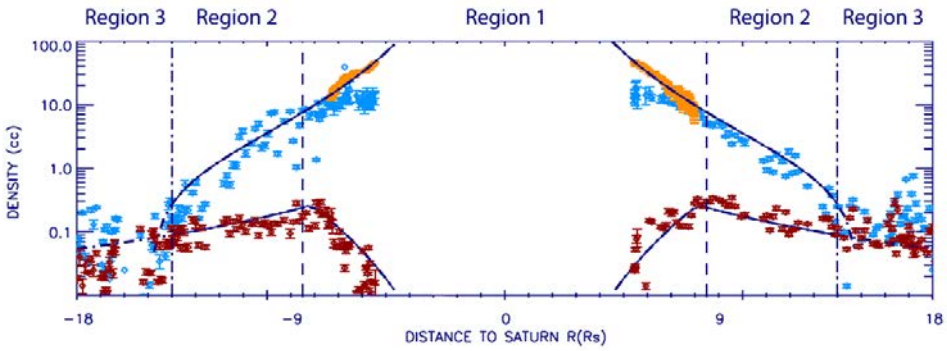

Figure 6.5: Median electron density profile versus orbital radius [33]

The description of the inner plasma distribution is even more complicated: it does not just follow a radial dependance but, as we will see, it is strongly influenced by the inclination with respect to the equator. Moreover, with Saturn having a very high rotational period of only less than 11 hours, the corotating plasma is subject to strong and rapid variations due to the changes in the conditions of illumination. Several radio occultations from Cassini were analyzed by Kilore et al. [34] and represented in charts that try to summarize the very complex behavior of plasmas in Saturn's inner ionosphere. Fig. 6.6

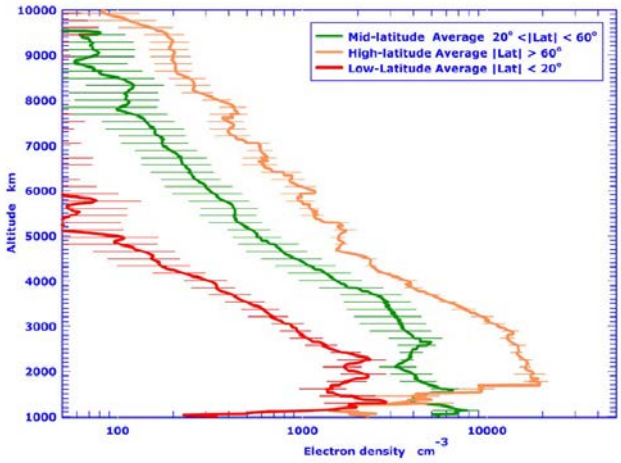

Figure 6.6: Median electron density profiles for different inclinations [34]

shows that the electron density increases with latitude: the trend appears to be evident and repeatable, regardless of other ambient conditions. Regardless of the latitude, the density profile seems to reach its maximum around 2000 km from the surface of the planet, and being as much as one order of magnitude higher in the high-latitude range than in the low-latitude range. Finally, fig. 6.7 shows that even within the same latitude range there are variations due to the different conditions of illumination. Strangely enough, in the case of mid-latitude regions, density profiles showed a higher density at dawn than at dusk, as opposed to the curves in fig. 6.7 for low-latitude

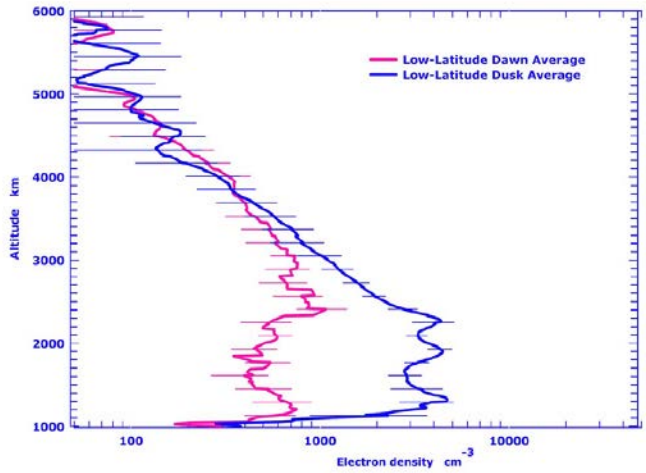

Figure 6.7: Median electron density profiles in dawn and dusk conditions [34]

regions: this is thought to be either due to the lack of more consistent data or some undetected plasma-injection phenomenon that happened during night-time [34]. In conclusion, it is clear that the choice of the orbit and the time at which the satellite reaches its closest approach to the planet are of vital importance in order to obtain the most desirable plasma density levels and perform the capture procedure successfully.

6.2.4 Preliminary Tether Design

This section will present the approach developed and followed by Sanmartín and Lorenzini, together with their coauthors in [28, 29], to give a preliminary estimate of mass and dimensions of a tether system that could effectively perform a planetary capture. In order to do so, the Lorentz drag needs to be able to perform a work $|W_d|$ to reduce the eccentricity from a hyperbolic value $e_h > 1$ to an elliptic value $e_e < 1$. The specific energy of an orbit can easily be expressed as a function of the eccentricity and the periapse radius

[6]:

$$\epsilon_i = \frac{\mu}{2r_p}(e_i - 1)$$

Remembering that for a hyperbolic orbit the specific energy is a function of the excess speed $\epsilon_h = v_\infty^2/2$, and that the periapse radius does not vary during the dragged arc (in first approximation), allows to express the drag work as [29]:

$$|W_d| = M_{S/C}\frac{v_\infty^2}{2} \cdot \frac{e_h - e_e}{e_h - 1} \Rightarrow \frac{|W_d|}{m_t v_\infty^2/2} = \frac{M_{S/C}}{m_t} \cdot \frac{e_h - e_e}{e_h - 1}$$

The rearranged expression on the right hand side is particularly useful because it reduces the problem to a limited number of dimensionless coefficients:

- $\frac{M_{S/C}}{m_t}$: it is the ratio between the spacecraft's mass and the tether mass;
- $\frac{e_h - e_e}{e_h - 1}$: it depends on the eccentricities before and after the dragged arc; e_h is usually known and very close to 1: $e_h - 1 \to 0$;
- $\frac{|W_d|}{m_t v_\infty^2/2}$: it is the dimensionless drag work, and it contains all the dynamic effects of the drag force on the spacecraft's trajectory.

The last term can be expressed as the product of dimensionless factors as follows [28]:

$$\frac{|W_d|}{m_t v_\infty^2/2} = B_s^{*2} \cdot W_d^*$$

where [28]:

$$B_s^{*2} = \frac{\sigma_c B_s^2 a_s v_s}{2^{5/6}\rho_c v_\infty^2}$$

with σ_c and ρ_c being the tether's conductivity and density respectively, and the subscripts 's' referring to values at stationary orbit. The derivation of the term W_d^* is much more elaborate and is explained in detail in [28]; for the purpose of this work it will suffice to say that the drag is calculated along a parabolic trajectory: with the eccentricity being very close to 1 (before and after the dragged arc) the error committed is small [29]. The orbit is assumed

to be equatorial and prograde, with the magnetic field $\vec{\boldsymbol{B}}$ perpendicular to the orbital plane and to the tether. The analysis leads to [28]:

$$W_d^* = 2{r_M^*}^{8/3} \int_1^{r_M^*} \frac{(r_M^* - r^*)dr^*}{{r^*}^6\sqrt{r^* - 1}} \cdot < i_{av} \cos^2 \phi >$$

with r_M defined in section 6.2.1 and r^* being the dimensionless radius $r^* = r/r_P$; i_{av} is the dimensionless current from section 6.2.2 and ϕ is the angle between the direction of the tether and the perpendicular to the radius-vector. When applying this theory to Saturn, as opposed to the case of Jupiter which was originally analysed in [28], it is clear that the significantly weaker magnetic field of Saturn poses a challenge to the capture procedure because of the dependance from B_s^2. This capture can be facilitated by injecting the spacecraft into a retrograde orbit, therefore having a much higher relative speed to the corotating plasma [29]; furthermore, the weaker interaction with the magnetic field produces a smaller force $\vec{\boldsymbol{F}}$, avoiding the spinning of the tether (otherwise necessary to counteract tether bowing), which is here assumed to lie along the local vertical ($\phi =$ const) [29]. The new expression for W_d^* takes the form [29]:

$$W_d^* = 2{r_M^*}^{8/3} \int_1^{\infty} \frac{(r_M^* + r^*)dr^*}{{r^*}^6\sqrt{r^* - 1}} \cdot < i_{av} >$$

Assuming the periapse to be very close to the surface of Saturn and the hyperbolic excess speed to be that of a non-thrust transfer orbit after a Jupiter flyby ($r_P \approx R_S$ and $v_\infty \approx 2.5$) leads to:

$$\frac{e_h - e_e}{e_h - 1} \cdot \frac{M_{S/C}}{m_t} =< i_{av} > \cdot 6.13$$

At periapse, the characteristic length defined above is $L_{ch} \approx 26$ km; designing the tether to be 52 km long leads to $i_{av} = 0.5$ at periapse, where the magnetic field is at its strongest value. Assuming also, as in first approximation, that the final orbit be exactly parabolic ($e_e = 1$) provides:

$$\frac{M_{S/C}}{m_t} \approx 3$$

which is comparable to the values for a Jupiter application [29]. For a spacecraft mass of 1000 kg this leads to a tether mass $m_t = 333$ kg, which in the case of aluminium provides $w = 24$ cm for $h = 10^{-2}$ mm.

We want now to analyse the possible benefits of reducing the hyperbolic excess speed in comparison to the results that have previously been calculated in [29]: the dependance from v_∞ is clear in the expression for B_s^{*2}. A lower v_∞ results in a value for the eccentricity that will be closer to unity; specifically, maintaining in both cases the hypothesis $r_P \approx R_S$ we obtain $e_h^I = 1.009930$ for $v_\infty^I = 2.5$ km/s and $e_h^{II} = 1.001589$ for $v_\infty^{II} = 1$ km/s. The reference value $v_\infty = 1$ km/s has been chosen for a conservative analysis, even though the relative speed, as it has been shown previously, can be reduced to a lower value. We assume that none of the parameters involved change besides the dimensions of the tether l and w: as a result of this assumption, the characteristic length L_{ch} stays unchanged as well as the result of the integral in the expression for W_d^*, which was calculated with the hypothesis of the orbits being parabolic. A comparison between the cases I and II with different values for v_∞ leads to the following equation:

$$\frac{\frac{e_h^I - e_e^I}{e_h^I - 1} \cdot \frac{1}{m_t^I}}{\frac{e_h^{II} - e_e^{II}}{e_h^{II} - 1} \cdot \frac{1}{m_t^{II}}} = \frac{< i_{av}^I >}{< i_{av}^{II} >} \cdot \frac{1}{\kappa}$$

with $\kappa = \left(v_\infty^I / v_\infty^{II}\right)^2 = 6.25$ with the aforementioned values. The possible improvements to the capture procedure seem to be two:

- improving the eccentricity ratio to obtain a lower e_e;
- reduce the tether mass m_t.

Reducing the post-capture eccentricity

Having a reduced eccentricity value for the captured elliptic orbit would result beneficial, as it would make the mission less likely to end with the

spacecraft not captured by the planet and therefore flying aimlessly in the deep space. Unfortunately, it can be shown analytically that reducing v_∞ does not improve e_e by a factor that is worth the struggle. Reiterating some of the aforementioned expressions for the specific orbital energy it is possible to express the eccentricity of a hyperbolic trajectory as:

$$e_h = \frac{r_P v_\infty^2}{\mu} + 1$$

Substituting this expression into the previous one leads to:

$$\frac{\frac{e_h^I - e_e^I}{\frac{r_P {v_\infty^I}^2}{\mu} + 1 - 1} \cdot \frac{1}{m_t^I}}{\frac{e_h^{II} - e_e^{II}}{\frac{r_P {v_\infty^{II}}^2}{\mu} + 1 - 1} \cdot \frac{1}{m_t^{II}}} = \frac{< i_{av}^I >}{< i_{av}^{II} >} \cdot \frac{1}{\kappa}$$

$$\frac{e_h^I - e_e^I}{e_h^{II} - e_e^{II}} \cdot \frac{1}{\kappa} = \frac{1}{\kappa} \Rightarrow \Delta e^I = \Delta e^{II}$$

This means that the final eccentricity only diminishes because the initial eccentricity e_h is, in the second case, slightly lower (the total decrement is less than 1%). This is motivated by the fact that the work of the Lorentz force is the same, acting along the same parabolic trajectory. It is in fact possible to reformulate the equations to reach the correlation:

$$\Delta\epsilon = \frac{\mu}{2r_P}\Delta e$$

Reducing the tether mass

Reducing the tether mass m_t is definitely of great interest for the entire mission: assuming to have a constant space mass $M_{S/C}$ in both cases, a lower tether mass allows for a higher mass fraction to be utilized for payload. The two parameters that are object of the optimization are, as previously said, length and width; the thickness is kept constant as well as the material density. The calculations from previous sections remain valid, providing a characteristic length of $L_{ch} = 26$ km at periapse. We want the tether to

be at most as long as it is in the first case analyzed (52 km), but preferably shorter: according to figure 6.2 this requirement is fulfilled in the range where the i_{av} current is a linear function of the ratio L/L_{ch}, which in the case of a constant characteristic length translates into $i_{av} \propto l$. Moreover, in this analysis we assume that the final orbit be barely elliptical ($e_e \to 1$) so that the eccentricity ratios equal 1. These considerations result in:

$$\frac{m_t^I}{m_t^{II}} = \kappa \cdot \frac{l^{II}}{l^I}$$

where κ is the same as in the previous case. Expressing the tether mass as $m_t = \rho l w h$ leads to the ultimate:

$$\kappa \frac{w^{II}}{w^I} \left(\frac{l^{II}}{l^I} \right)^2 = 1$$

which can be interpreted as follows: in the case with a reduced hyperbolic excess velocity, the capture is performed equivalently by an electrodynamic tether that is κ times narrower ($w^I = \kappa w^{II}$) or $\sqrt{\kappa}$ times shorter ($l^I = \sqrt{\kappa} l^{II}$). Combination of the two are also possible, reducing both the dimensions, following the plots in fig. 6.8 obtained reformulating the last equation. With the mass m_t being directly proportional to both w and l, the best solution to reduce the total tether mass would be to leave the length unchanged and reduce the width by a factor κ. Unfortunately, with the tether width being of the order of magnitude of centimeters, it might not be safe to scale it down too much to avoid the rupture of the tether. In this circumstance, the width can be reduced to the minimum safe value, while a fraction of κ can be 'implemented' in a reduction of the tether length l.

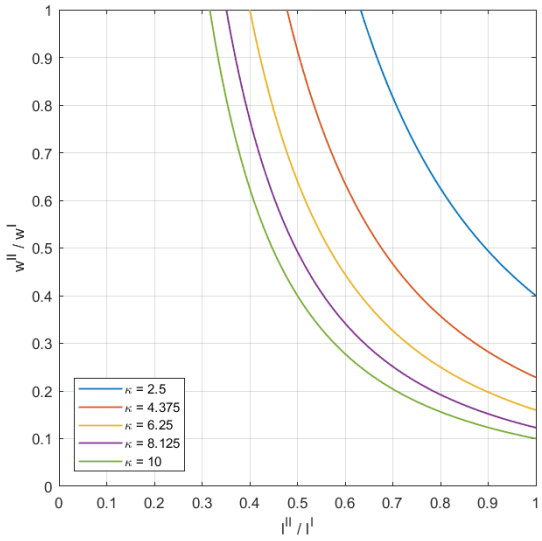

Figure 6.8: w^{II}/w^{I} versus l^{II}/l^{I} for different κ values

Chapter 7

Conclusions and future work

This work presented the preliminary design of a tethered mission to Saturn. Initially, *Differential Evolution Algorithms* have been presented as a well established and reliable means to prune the space of viable solutions in the search for optimal launch windows. A mathematical theory has been laid out to incorporate a thrust arc in the Jupiter-to-Saturn transfer orbit to optimize the trajectory: the theory provides the optimal orientation for the thrust angle and the *Gaussian Planetary Equations* allow to calculate the evolution of the keplerian parameters, together with the spacecraft's position and velocity vectors, along the thrust arc. The main characteristics of the mission are resumed in the following points:

- it is a small mission of 1000 kg, much less than the Cassini/Huygens (wet mass $\approx$ 5600 kg [16]);
- it involves a flyby around Jupiter: wether the flyby will be powered or unpowered, is yet to be determined;
- the spacecraft incorporates a low-thrust engine, which realizes a thrust arc *in the final part* of the transfer orbit from Jupiter to Saturn: this allows for a reduction of the hyperbolic excess speed at the encounter with Saturn to values lower than 1 km/s;

- the capture procedure is performed by an *electrodynamic tether*, whose design is improved thanks to the lower hyperbolic excess speed, allowing for a significant total mass fraction to be dedicated to payload.

Many aspects of the mission design need to be studied further in the details. Future studies will be conducted in order to present a complete and fully structured proposal. Some of the aspects that will be explored in the future are the following:

- detailed formulation of the launch window, with specific focus on the corrective maneuvers to be implemented to reach Jupiter with the desired conditions (see section 5.4);
- formulation of a realistic mass flow expelled by the electric thruster and the impact it has on the acceleration perceived by the spacecraft, with an expected modification in the thrust arc;
- more accurate analysis of the hyperbolic trajectory of the spacecraft entering Saturn's sphere of influence, accounting for the planet's inclination with respect to the equatorial plane and the non-perpendicularity of the local magnetic field to the S/C's trajectory;
- further improvement of the tether design, with the aim of using it as a thruster to explore the Saturnian moon system, following the trail presented in [35].

It ought to be mentioned that there is some skepticism in the scientific community about the reliability of tether systems, especially when performing a capture procedure that only has one chance to be executed properly. When passing through the hyperbolic perigee, any malfunction in the deployment of the tether or in the electric circuit might lead to an inefficient dragged arc and, as a consequence, the departure of the spacecraft from the planet. Nevertheless, the reduced relative speed at the encounter with Saturn has

a positive impact on the mission even in the hypothesis of using a chemical thruster to perform the capture procedure. Figure 7.1 shows that with $v_\infty = 1$ an elliptic, close orbit can be acquired with Δv's smaller than 100 m/s, therefore significantly easier to deal with than the 622 m/s required by the Cassini spacecraft [7, 16].

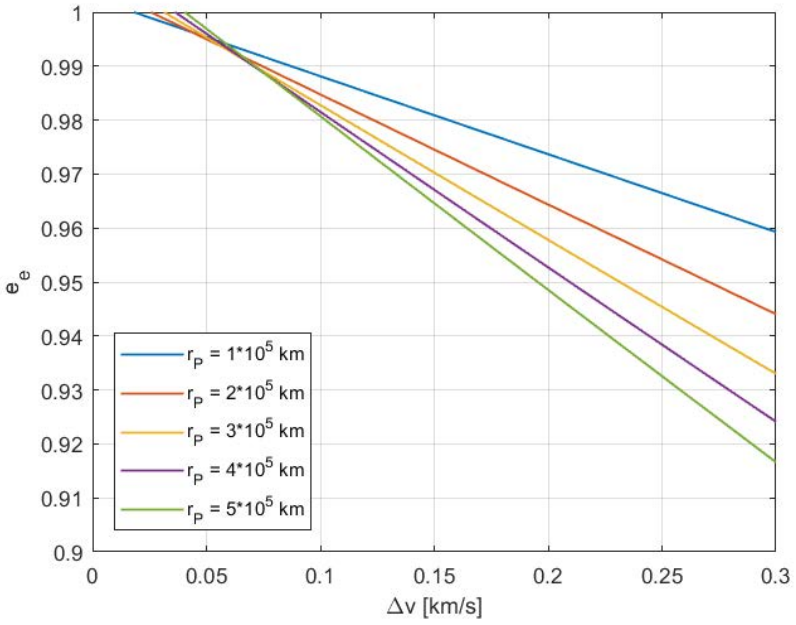

Figure 7.1: Final eccentricity e_e versus capture Δv, with $v_\infty = 1$

Despite the aspects that still need adjustment, the work conducted so far has proven to give encouraging results, which could lead the way to the exploration of the Gas Giants through smaller and cheaper missions in the future.

Bibliography

[1] Cynthia B Phillips and Robert T Pappalardo. Europa clipper mission concept: exploring Jupiter's ocean moon. *Eos, Transactions American Geophysical Union*, 95(20):165–167, 2014. ISSN 0096-3941. doi: 10.1002/2014eo200002.

[2] JJ Plaut, S Barabash, L Bruzzone, M Dougherty, C Erd, L Fletcher, R Gladstone, O Grasset, L Gurvits, P Hartogh, et al. Jupiter icy moons explorer (JUICE): science objectives, mission and instruments. In *45th Lunar and Planetary Science Conference*, page 2717, 2014.

[3] Frank Postberg, Sascha Kempf, Jürgen Schmidt, N Brilliantov, Alexander Beinsen, Bernd Abel, Udo Buck, and Ralf Srama. Sodium salts in E-ring ice grains from an ocean below the surface of Enceladus. *Nature*, 459(7250):1098, 2009. ISSN 0028-0836. doi: 10.1038/nature08046.

[4] Jonathan I Lunine. Ocean worlds exploration. *Acta Astronautica*, 131: 123–130, 2017. ISSN 0094-5765. doi: 10.1016/j.actaastro.2016.11.017.

[5] Stephen Kemble. *Interplanetary mission analysis and design*. Springer Science & Business Media, 2006.

[6] Howard D Curtis. *Orbital mechanics for engineering students*. Butterworth-Heinemann, 2013.

[7] Troy Goodson, Donald Gray, Yungsun Hahn, and Fernando Peralta. Cassini maneuver experience: Launch and early cruise. In *Guidance, Navigation, and Control Conference and Exhibit*, page 4224, 1998. doi: 10.2514/6.1998-4224.

[8] Rainer Storn and Kenneth Price. Differential evolution–a simple and efficient heuristic for global optimization over continuous spaces. *Journal of global optimization*, 11(4):341–359, 1997.

[9] Shuguang Zhao, Xu Wang, Liang Chen, and Wu Zhu. A novel self-adaptive differential evolution algorithm with population size adjustment scheme. *Arabian Journal for Science and Engineering*, 39(8):6149–6174, 2014. ISSN 1319-8025. doi: 10.1007/s13369-014-1248-7.

[10] A.K. Qin and P.N. Suganthan. Self-adaptive differential evolution algorithm for numerical optimization. In *2005 IEEE Congress on Evolutionary Computation*. IEEE, 2005. doi: 10.1109/cec.2005.1554904.

[11] Janez Brest, Sao Greiner, Borko Boskovic, Marjan Mernik, and Viljem Zumer. Self-adapting control parameters in differential evolution: A comparative study on numerical benchmark problems. *IEEE transactions on evolutionary computation*, 10(6):646–657, 2006. ISSN 1089-778X. doi: 10.1109/tevc.2006.872133.

[12] Jouni Lampinen, Ivan Zelinka, et al. On stagnation of the differential evolution algorithm. In *Proceedings of MENDEL*, pages 76–83, 2000.

[13] Sam Wagner and Bong Wie. Hybrid algorithm for multiple gravity-assist and impulsive delta-v maneuvers. *Journal of Guidance, Control, and Dynamics*, 38(11):2096–2107, 2015. ISSN 0731-5090. doi: 10.2514/1.g000874.

[14] Richard H Battin. *An Introduction to the Mathematics and Methods of*

Astrodynamics, revised edition. American Institute of Aeronautics and Astronautics, 1999.

[15] Jacob A Englander, Bruce A Conway, and Trevor Williams. Automated mission planning via evolutionary algorithms. *Spaceflight Mechanics*, 35:1878–1887, 2012. ISSN 0731-5090. doi: 10.2514/1.54101.

[16] Fernando Peralta and JC Smith Jr. Cassini trajectory design description. 1993.

[17] David A Vallado. *Fundamentals of astrodynamics and applications*, volume 12. Springer Science & Business Media, 2001.

[18] Jesús Peláez Álvarez. Optimizar la captura con low thrust. Universidad Politécnica de Madrid, 2018.

[19] Elaine M Petro and Raymond J Sedwick. Survey of moderate-power electric propulsion systems. *Journal of Spacecraft and Rockets*, 54(3): 529–541, 2017. ISSN 0022-4650. doi: 10.2514/1.a33647.

[20] Jonathan Van Noord. Lifetime assessment of the next ion thruster. In *43rd AIAA/ASME/SAE/ASEE Joint Propulsion Conference & Exhibit*, page 5274, 2007. doi: 10.2514/6.2007-5274.

[21] Eric J Pencil. Recent electric propulsion development activities for nasa science missions. In *2009 IEEE Aerospace conference*, pages 1–9. IEEE, 2009. doi: 10.1109/aero.2009.4839593.

[22] Robert G Lange and Wade P Carroll. Review of recent advances of radioisotope power systems. *Energy Conversion and Management*, 49 (3):393–401, 2008. ISSN 0196-8904. doi: 10.1016/j.enconman.2007.10.028.

[23] Daniel Champier. Thermoelectric generators: A review of applications. *Energy Conversion and Management*, 140:167–181, 2017. ISSN 0196-8904. doi: 10.1016/j.enconman.2017.02.070.

[24] Julien Vaudolon, Vanessa Vial, Nicolas Cornu, and Idris Habbassi. PPS®X00 hall thruster development at Safran. In *International Astronautical Congress (IAC)*, Bremen, Germany, October 2018. International Astronautical Federation (IAF).

[25] Mario L Cosmo and Enrico C Lorenzini. *Tethers in space handbook*. Smithsonian Astrophysical Observatory, Cambridge, Massachusetts, 1997.

[26] Enrico C Lorenzini. Lecture notes from the 'Astrodynamics' course. University of Padua, 2017.

[27] Juan Ramón Sanmartín and Enrico C Lorenzini. Exploration of outer planets using tethers for power and propulsion. *Journal of Propulsion and Power*, 21(3):573–576, 2005. ISSN 0748-4658. doi: 10.2514/1.10772.

[28] Juan Ramón Sanmartín, Mario Charro, Enrico C Lorenzini, Henry B Garrett, Claudio Bombardelli, and Cristina Bramanti. Electrodynamic tether at Jupiter—I: Capture operation and constraints. *IEEE Transactions on Plasma Science*, 36(5):2450–2458, 2008. ISSN 0093-3813. doi: 10.1109/tps.2008.2002580.

[29] Juan Ramón Sanmartín, Jesús Peláez Álvarez, and Ignacio Carrera-Calvo. Comparative Saturn-Versus-Jupiter tether operation. *Journal of Geophysical Research: Space Physics*, 123(7):6026–6030, 2018. ISSN 2169-9380. doi: 10.1029/2018ja025574.

[30] Juan Ramón Sanmartín Losada, Enrico C Lorenzini, and Manuel Martínez Sánchez. Electrodynamic tether applications and constraints. 47:442–456, 2010. ISSN 0022-4650. doi: 10.2514/1.45352.

[31] E S Belenkaya, I I Alexeev, V V Kalegaev, and M S Blokhina. Definition of Saturn's magnetospheric model parameters for the Pioneer 11 flyby. *Annales Geophysicae*, 24(3):1145–1156, 2006. ISSN 1432-0576. doi: 10.5194/angeo-24-1145-2006.

[32] A M Persoon, D A Gurnett, W S Kurth, G B Hospodarsky, J B Groene, P Canu, and M K Dougherty. Equatorial electron density measurements in saturn's inner magnetosphere. *Geophysical research letters*, 32(23), 2005. ISSN 0094-8276. doi: 10.1029/2005gl024294.

[33] P Schippers, M Blanc, N André, I Dandouras, GR Lewis, LK Gilbert, AM Persoon, N Krupp, DA Gurnett, AJ Coates, et al. Multi-instrument analysis of electron populations in Saturn's magnetosphere. *Journal of Geophysical Research: Space Physics*, 113(A7), 2008. ISSN 0148-0227. doi: 10.1029/2008ja013098.

[34] AJ Kliore, AF Nagy, EA Marouf, A Anabtawi, E Barbinis, DU Fleischman, and DS Kahan. Midlatitude and high-latitude electron density profiles in the ionosphere of Saturn obtained by Cassini radio occultation observations. *Journal of Geophysical Research: Space Physics*, 114 (A4), 2009. ISSN 0148-0227. doi: 10.1029/2008ja013900.

[35] Juan Ramón Sanmartín and Jesús Peláez. Planetary exploration of Saturn moons Dione and Enceladus. In *8th European Conference for Aeronautics and Space Sciences (EUCASS)*, July 2019.